AN ABSTRACT OF THE THESIS OF

Keith R. Davis for the degree of Master of Science in Mechanical Engineering presented on December 10, 2007.

Title: Proportional Integral Derivative Control of an Oil-heated Fractal-like Branching Microchannel Desorber

Abstract approved:

John Schmitt Deborah V. Pence

A PID controller was designed to control the performance of an oil-heated fractal-like branching microchannel desorber for use in an ammonia-absorption refrigeration system. Both the amount and concentration of ammonia refrigerant generated at the desorber can be controlled by choosing the rectified circulation ratio as the controlled variable in a single-input single-output (SISO) system. The oil pump control voltage was chosen to be the controller input. System identification tests were performed to create a simple model of the dynamical relationship between rectified circulation ratio (f*) and oil pump control voltage for four different operating conditions. The dynamical relationship between f* and oil pump control voltage can be represented as a time delay two pole system with 84% accuracy. The models were used to simulate desorber performance and design PID controllers. The

closed loop response of the desorber under various operating conditions and controller combinations was simulated, and two promising controllers were tested on the desorber using an experimental flow loop. Additional tuning of the PID controller on the experimental loop resulted in a closed-loop response that had faster rise time and lower over-shoot than the simulated controllers. The gains of this controller are: k_p= 0.3, k_i= 0.003, and k_d = 2.0. The tuned controller controlled the desorber and regulated to the desired rectified circulation ratio under the four operating conditions studied. The closed-loop response of the desorber varied depending on the operating conditions and the f* value of the desorber. The controller was able to track desired f* signals with a settling time of approximately 10 minutes. Combinations of strong solution flow rate, oil temperature, and manifold pressure disturbances were introduced into the system to test the robustness of the controller. Strong solution flow rate disturbances produced the largest change in f*. All three types of disturbances were controlled with a settling time less than or approximately equal to the settling time observed during the tracking tests.

Proportional Integral Derivative Control of an Oil-heated Fractal-like Branching Microchannel Desorber

by

Keith R. Davis

A THESIS

submitted to

Oregon State University

in partial fulfillment of
the requirements for the
degree of

Master of Science

Presented December 10, 2007
Commencement June 2008

Master of Science thesis of Keith R. Davis presented on December 10, 2007.

APPROVED:

Co-Major Professor, representing Mechanical Engineering

Co-Major Professor, representing Mechanical Engineering

Head of the School of Mechanical, Industrial, & Manufacturing Engineering

---

Dean of the Graduate School

I understand that my thesis will become part of the permanent collection of Oregon State University libraries. My signature below authorizes release of my thesis to any reader upon request.

Keith R. Davis, Author

ACKNOWLEDGEMENTS

I would like to thank Dr. Deborah Pence for seeing the potential for this research and for providing me the opportunity to conduct it. Thank you to Dr. John Schmitt for the direction and help you provided in conducting this research and in writing this thesis. Also, thank you to Drs. Chiang and Liburdy for serving on my committee.

I would like to thank Greg Mouchka for training in using the experimental flow loop and fellow researchers Mario Apreotesi, Alex Tulchinsky, and Chris Stull for their help in preparing for and conducting tests in the lab.

Mostly, I would like to thank my wife Vanessa for her patience, faith, and support as I have struggled through this challenging task. Lastly, I thank God for His hand in my life, the opportunities I have been given, and his support in completing this work.

TABLE OF CONTENTS

Page

LIST OF FIGURES

LIST OF FIGURES (CONTINUED)

Figure Page

LIST OF TABLES

LIST OF APPENDICES

Page

LIST OF APPENDIX TABLES

NOMENCLATURE

VARIABLES AND PARAMETERS

f	Circulation ratio
f*	Rectified circulation ratio
f_{opt}^{*}	Optimal rectified circulation ratio
M	Number of replications
Q_D	Heat of desorption
Q_e	Heat of evaporation
W_P	Pump work
L	Channel length
W	Channel width
γ	Length ratio
β	Width ratio
$G(s)$	Plant transfer function
$G_c(s)$	Controller transfer function
$C(s)$	Controlled output
$R(s)$	Desired output
k_p	Proportional gain

k_d	Derivative gain
k_i	Integral gain
T	Temperature (K, °c), sampling rate, tuned controller
T_{sat}	Saturation Temperature (K, °c)
x	Ammonia concentration
P	Pressure (bar, psi)
P_{man}	Manifold Pressure
SV	Controller plant variable
$\dot{m}_{oil}$	Oil mass flow rate (g/min, g/s)
$u(t)$	System input
$y(t)$	System output
d_f	Dryness fraction
ET_{sw}	Mean switching time
$Ts_{98\%}$	98% settling time
$\tau_{\min}$	Minimum process time
G_r^E	Gibbs excess energy
S_x	Pooled standard deviation of the means
u_p	Precision error
u_b	Biased error
e	error
u	uncertainty

T_r Rise time

T_s Settling time

$\%OS$ Percent overshoot

SUPERSCRIPTS

xm Model order x

EXP Experimental system

L Liquid phase

SUBSCRIPTS

1 Strong solution

2 Desorbed vapor

2* Rectified vapor

3 Weak solution

3* Reflux solution

NC No controller

A Model A controller

C Model C controller

D Model D controller

E Model E controller

m Mixture

a Ammonia

w Water

Proportional Integral Derivative Control of an Oil-heated Fractal-like Branching Microchannel Desorber

1. INTRODUCTION

Absorption refrigeration cycles are receiving renewed interest as energy prices rise and Chlorofluorocarbons (CFC's) continue to be phased out. Absorption cycles are also being considered for applications requiring light weight compact cycle components. Fractal-like branching microchannels have been used in the design of a small compact desorber [1]. The method and ability to control the desorber performance are investigated in this study.

1.1. Refrigeration Cycles

An absorption refrigeration cycle has several advantages over a standard vapor compression cycle including the ability to operate using waste heat, reduced work input requirements, and quieter operation.

1.1.1. Overview

The standard vapor compression refrigeration cycle illustrated in figure 1.1 is well understood and used in numerous applications. In this cycle, beginning at the compressor, the working fluid is compressed to a higher pressure raising its temperature.

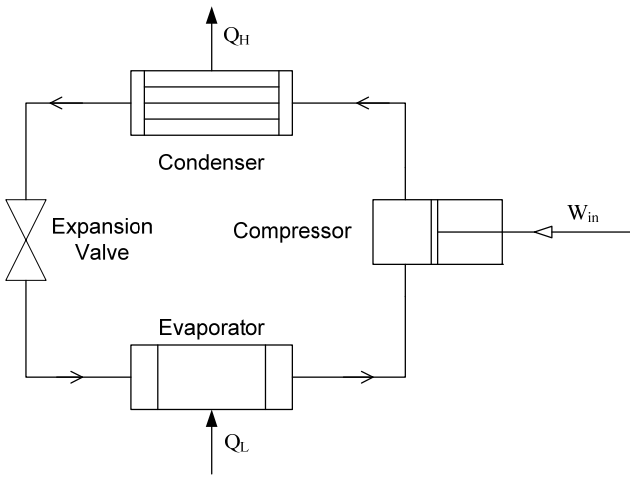

Figure 1.1: Standard vapor compression refrigeration cycle

The cycle rejects heat as the working fluid passes through the condenser. An expansion valve lowers the pressure and cools the working fluid, after which it passes through the evaporator where it receives heat as it cools the refrigerated space. An extensive overview of the topic can be found in [2] by Çengel and Boles.

1.1.2. Absorption Refrigeration Cycle

While not new, ammonia absorption refrigeration cycles are receiving increased interest since the refrigerant is a naturally occurring substance and does not contribute green house gases. An absorption refrigeration cycle is similar to the standard refrigeration cycle in the condenser, evaporator, and throttling valve. However, an absorption cycle uses a “chemical” compressor, as opposed to a mechanical compressor, to bring the refrigerant to the high side pressure. Figure 1.2 shows a schematic of an absorption refrigeration cycle. The chemical compressor is comprised of several parts: absorber, recuperator, desorber (generator), and rectifier (distiller). While the chemical compressor is more complex, it serves the same

purpose as the mechanical compressor: to bring the ammonia refrigerant to the high side pressure and a temperature greater than ambient. The flow of the ammonia refrigerant through the chemical compressor is best explained beginning at the absorber. Here ammonia gas is absorbed into an ammonia-water solution, weak in ammonia concentration. The resulting binary mixture, now more concentrated in ammonia, is subsequently pumped to a higher pressure. It then passes through the recuperator which preheats the solution, thus improving the coefficient of performance (COP) of the cycle. The desorber (generator) desorbs the solution creating an ammonia rich vapor. However, because the vapor pressure of water is not negligible with respect to ammonia, the ammonia rich vapor produced will still contain a certain portion of water vapor. As a result, the vapor is passed through the rectifier which condenses and removes much of the water vapor further increasing the ammonia vapor concentration. At this point the ammonia refrigerant has arrived at the same state it would have achieved had it passed through a mechanical vapor compressor.

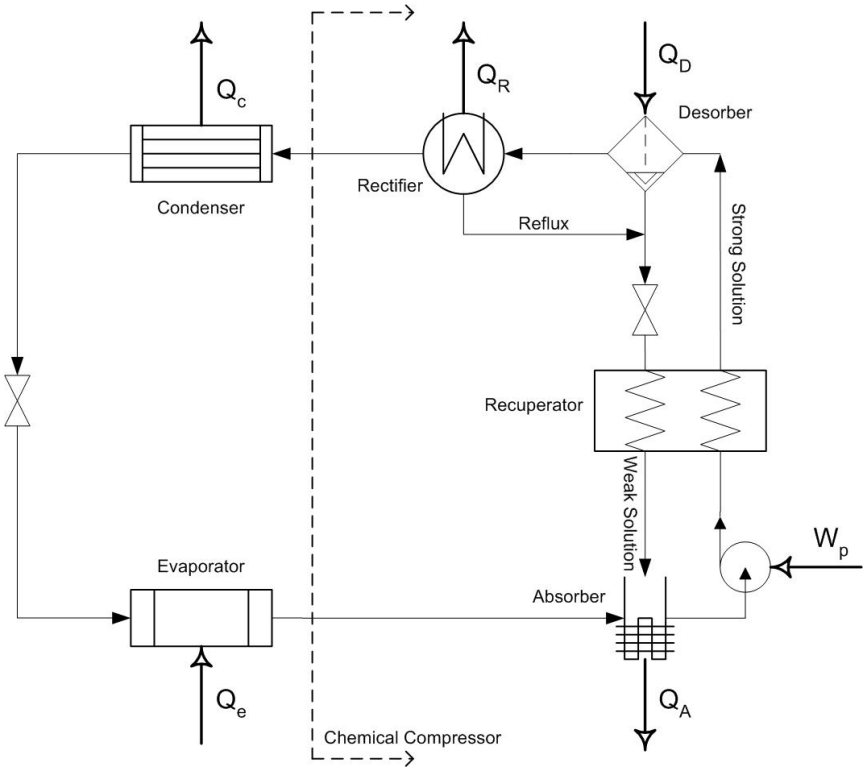

Figure 1.2: Absorption refrigeration cycle

The absorption cycle is beneficial because of the cycle's ability to operate using waste heat, represented as Q_D in Fig. 1.2. Additionally, the work at the pump in an absorption refrigeration cycle is much less than the work at the compressor of a standard refrigeration cycle. The COP for this system is defined as the ratio of the heat of evaporation (Q_e) to the heat of desorption (Q_D):

$$COP = \frac{Q_e}{Q_D}. \tag{0}$$

The pump work (W_P) can be neglected because it is an order of magnitude smaller than either Q_e or Q_D.

1.2. Current Trends

As energy prices increase absorption refrigeration cycles are also being considered for much smaller applications than those for which they have generally been used. Garimella [3] provides an example application of the use of an absorption refrigeration cycle for space conditioning of a recreational vehicle. Garrabrant [4] investigated using the waste heat from the exhaust of a diesel truck engine to run an absorption refrigeration cycle for cooling a refrigerated trailer pulled behind the truck, although heat supplied from the hot engine oil could also be used in an oil heated desorber. These types of cycle applications clearly require much smaller components than typical industrial applications. Size and weight reduction in refrigeration cycle parts can be achieved through the use of microchannels to increase heat and mass transfer coefficients. The drawback to the use of parallel microchannels is the significant increase in the pressure drop across the channels for a fixed flow rate, which results in a larger required pumping power.

1.2.1. Fractal-like Branching Microchannels

Inspired by the natural fractal-like patterns found in leaves and the mammalian cardiovascular system, branching fractal-like microchannels have been examined since 1997 [5] . In contrast to the large pressure drops in parallel microchannels, Pence [6] showed that a fractal-like branching microchannel network has a 30% lower pressure drop than a parallel microchannel configuration with the same total convective surface area for the same flow rate. While yielding a significantly lower

pressure drop, a fractal-like microchannel arrangement also had a 30°C lower wall temperature.

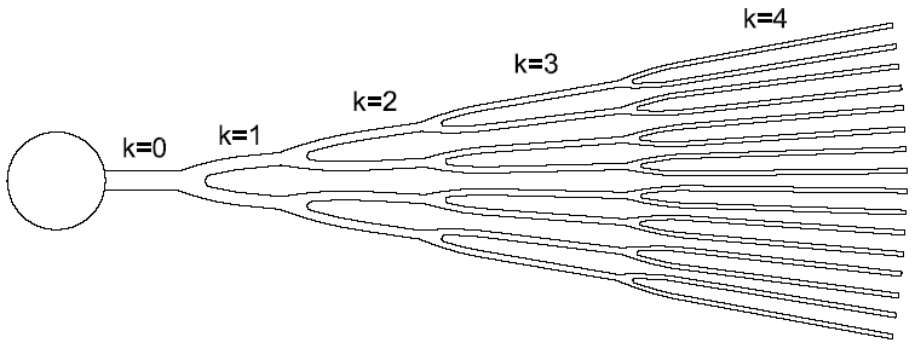

Fig. 1.3: A representation of one sixteenth of the microchannel array with length and width ratios used in this study (used with permission, [1])

The fractal-like microchannels investigated in this and previous studies have a channel length (L) and width (W) at each level which adhere to the following scaling relationships, respectively:

$$\frac{L_{k+1}}{L_k} = \gamma , \tag{1}$$

$$\frac{W_{k+1}}{W_k} = \beta . \tag{2}$$

In equations (1) and (2) k refers to a branching level as illustrated in figure 1.3. In figure 1.3 and in the fractal-like branching channels used in this study, $\gamma = 1.4$ and $\beta = 0.71$.

The high heat and mass transfer rates coupled with the lower pressure drop penalty of a fractal-like branching microchannel configuration provide significant potential for reducing absorption cycle component size and weight.

1.3. Fractal-like Branching Desorber

Recently Mouchka [1] incorporated fractal-like branching microchannels in the design of a desorber for an absorption refrigeration cycle. The desorber design developed can be classified as a co-flow desorber because the exiting vapor is in equilibrium with the ammonia weak solution exiting the desorber. This is in contrast to popular desorber designs which are counter-flow, in which the exiting vapor is in equilibrium with the ammonia rich solution entering the desorber. Co-flow desorbers are in general less desirable because the ammonia vapor stream requires more rectification to reach pure ammonia as compared to counter flow desorbers. However, the significant size reduction and high heat transfer coefficient obtainable through the use of fractal-like branching microchannels make a fractal-like branching microscale desorber an innovative design in situations where the size and/or weight of cycle components is critical to the intended application. The fractal-like branching desorber studied in this research is oil heated and explained in detail in chapter 3.

1.4. Cycle and Desorber Control

Using an absorption refrigeration system in new applications such as those detailed previously will result in the cycle operating in a transient state much more frequently than cycles in industrial operations. Because absorption refrigeration

systems operating in the transient regime often have a cycle performance below the steady state performance [7], cycle control presents an opportunity to improve performance. Methods for increasing the COP by controlling the cycle operation to improve the efficiency of the system during transient operation remain an area of active research. Most methods focus on controlling the heat input into the desorber since it determines the amount and quality of refrigerant vapor produced, thereby having a direct effect on the refrigeration cycle performance. The parameters of the absorption refrigeration cycle which are most suitable to serve as the controlled variable remains the focus of ongoing research. However, the desorber should be controlled to maximize the ammonia vapor generation and vapor concentration. This is difficult because the vapor generation and concentration have an inverse relationship. Controller design will depend on the dynamical relationship between the chosen input(s) and output(s). The desorber dynamics are highly complex by nature, involving heat transfer to a three dimensional flow and boiling of binary mixtures, all of which depends on desorber geometry. It is difficult, if not impossible in some cases, to derive an analytical relationship between the input and output quantities from first principles. While a more complex Multiple-Input Multiple-Output (MIMO) system model may represent the dynamics better than simpler Single-Input Single-Output (SISO) models, these systems require more complicated controllers and more computing power for implementation. Controllers for SISO systems are much simpler to design and implement. Unfortunately, controlling two variables such as vapor generation and vapor concentration would prohibit the use of

a SISO system model. Yet, a single variable exists for this system that enables the use of a SISO model for control purposes. This variable is known as the rectified circulation ratio and is explained in further detail in sections 4.1 and 4.2.

1.4.1. Proportional Integral Derivative Controller

Controller design for a SISO system begins by utilizing the simplest controller and adding additional complexity as needed to obtain desired performance. The proportional-plus-integral-plus-derivative (PID) controller is the simplest form of controller for a SISO system. Figure 1.4 shows the block diagram of the parallel form of a PID controller in the Laplace domain. It consists of three terms: 1, $\frac{1}{s}$, & s which act on the error, the integral of the error, and the derivative of the error, respectively. Each term includes a variable k, with subscripts denoting which term the gain is acting on. $G(s)$ represents the dynamics of the plant or system to be controlled, which is the desorber for this study. $G_c(s)$, denoted by the dashed box, represents the PID controller, $C(s)$ is the controlled output, and $R(s)$ represents the desired value of the output.

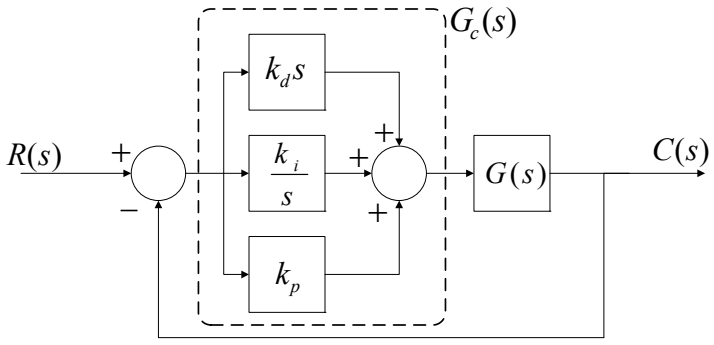

Fig. 1.4: Block diagram of the parallel form of a PID controller

The equation for the PID controller is:

$$G_c(s) = k_p + \frac{k_i}{s} + k_d s\,, \tag{2}$$

which can be rewritten

$$G_c(s) = K_c^{'}(1 + \frac{1}{\tau_I^{'} s} + \tau_D^{'} s)\,, \tag{3}$$

where

$$K_c^{'} = k_p\,; \quad K_c^{'}\tau_D^{'} = k_d\,; \quad \frac{K_c^{'}}{\tau_I^{'}} = k_i\,. \tag{4}$$

PID controller design requires determining the gains for each term to stabilize the system and obtain the desired operating performance. Changing the gains of the controller can drastically affect the response of the closed loop system. While many different theoretical tuning rules exist for selecting the PID gains, additional tuning on the physical system is often required in practice.

1.5. Scope and Objectives

The scope of this work is to design and test a controller to regulate the desorber output around a desired set point, and to determine controller robustness to variations in cycle operating conditions. Objectives supporting the attainment of these overall goals are:

1. to generate a mathematical model of the dynamic relationship between oil pump control voltage and rectified circulation ratio for various operating conditions,

2. to use the model to design a controller which will control the rectified circulation ratio, and
3. to implement the controller in the experimental setup and evaluate controller performance for a range of cycle operating conditions.

2. LITERATURE REVIEW

The focus of this research is the design of a control scheme for regulation of the rectified circulation ratio of a fractal-like branching microchannel desorber using the oil flow rate as the control input. Below is a review of research relevant to this study.

2.1. Fractal-like Branching Networks

Pence [8] used scaling laws on efficient transport in biological systems modeled in [5] (e.g. circulatory system) to design heat sinks with a branching network of microchannels that decrease in size with each branching level. Because the number of microchannels increases with each branching level the net affect is an increase in flow area for each branching level. Subsequent analysis of a one-dimensional model of the flow network illustrated that fractal-like branching networks offered a 30% reduction in pressure drop when compared to a straight channel flow network with identical flow area and pumping power [6]. The model also showed the branching network to have a wall surface temperature 30% lower for the same heat flux. For two phase flow in fractal-like branching microchannels, Daniels [9] predicted reduced pressure drops and pumping than would be required for flow through similar parallel microchannel arrays.

2.2. Desorption

Desorption is the process of producing a vapor concentrated in only one substance from a liquid that is a mixture of two substances, i.e. a binary liquid. It differs from evaporation because, as a binary liquid evaporates the concentration of the two substances in the vapor after evaporation is the same as in the liquid before

evaporation. Desorption produces a vapor that is more concentrated in one of the two substances.

In its simplest form any desorber design can be viewed as a heat exchanger in which heat is supplied to desorb a refrigerant from a binary mixture. Desorber design greatly influences the effectiveness of the desorption process with the clearest example being the difference between counter-flow and co-flow desorbers explained in the introduction. Garimella found that a counter-flow design increased the cycle COP by almost 16% over a co-flow design in one configuration of an absorption refrigeration system (ARS) [3]. Despite the performance improvements obtained through desorber design modifications, few investigations have produced a design methodology for desorption components. Kang proposed a design methodology for the major components of an absorption heat pump including the desorber [10]. In that work, the desorber consists of two counter-current falling film flows in a vertical fluted tube. Concentration, mass, and energy balances utilized in conjunction with diffusion and heat transfer equations were used to arrive at a model which drives the design.

One reason such scant literature on desorber design methodology exists is because there continue to be many new desorber designs investigated that cannot be analyzed by the method proposed by Kang [10]. Of those that cannot, Garrabrant [4] studied a cycle that uses a plate-fin generator design in an ammonia/water absorption refrigeration system designed specifically for truck transport refrigeration. The generator receives heat from hot hydronic fluid flowing through the generator. While

rather vague in explanation of the desorber design Garrabrant provides sufficient detail to eliminate any use of a falling film modeling approach.

Garimella studied two gas fired absorption systems for use in recreational vehical space conditioning, one using ammonia/water and the other using ammonia/NaSCN [3]. These gas fired systems supplied the generator heat from flue gases. The generator design is a circular array of tubes enhanced with fins around which the flue gases flow, transferring heat. Ammonia vapor is desorbed from the solution as it flows through the tubes. As mentioned earlier, Garimella found that the counter-flow generator operation increased the cycle COP by approximately 16% over the co-flow operation. Garimella's conclusion that "the system COP depends strongly on the generator configuration" succinctly describes the motivation for investigating new desorber configurations; to improve the attainable absorption refrigeration cycle COP.

2.3. Fractal-Like Branching Desorber

The use of a branching fractal-like flow network in a desorber is another new design which is promising for many applications because of the lower pressure drop penalty across the flow network. Cullion [11] demonstrated the feasibility of using a branching fractal-like network for desorption by attaching a nichrome heater to a fractal-like branching heat sink to supply heat and desorb ammonia water flowing through the channels. The rate of desorption was measured as a function of the applied heat flux and the strong solution flow rate. Cullion found that both the rate of desorption and the water content of the ammonia vapor produced increased with an

increase in applied heat flux for a fixed strong solution flow rate. Mouchka [1] further investigated the heat transfer and desorption rates of a fractal-like branching heat exchange desorber and identified desirable operating conditions. In the work, the desorber studied was oil heated and designed with fractal-like branching networks on both the oil and ammonia sides of the desorber separated by a thin plate. Mouchka's results agreed with those found by Cullion; vapor mass flow rate increases with applied heat and the vapor mass fraction decreases with applied heat. Mouchka also found that the vapor mass flow rate is minimally dependent on strong solution flow rate into the desorber and that vapor mass fraction increased with increasing strong solution flow rate. Additionally, Mouchka's research demonstrated that heat transfer between the oil and ammonia increases with increasing oil flow rate and oil temperature but was minimally dependent to changes in strong solution flow rate. Perhaps most relevant to this study, Mouchka showed that for a given desorber-rectifier configuration, including desorber design and cycle operating state points, a minimum required heat of desorption exists. This minimum required heat value corresponds to a specific desorber/rectifier circulation ratio (f^*) called the optimal circulation ratio, f^*_{opt} . Thus, for any set of operating conditions, operating the desorber at the optimal circulation ratio is equivalent to maximizing the desorber performance for those conditions in the given system.

2.4. The Motivation for Control

Nearly all refrigeration systems require control, otherwise the system would constantly operate at maximum capacity thereby cooling the chilled space beyond

the desired temperature. Traditional control designs have utilized an “on-off” approach which results in poor temperature control, limited operational conditions, reduced equipment life and increased energy consumption [34]. As a result, new approaches for absorption refrigeration system control remain the subject of many investigations. Didion in [7] investigated the difference between partial load performance and steady state performance of an absorption cycle water chiller in a laboratory setting. The on/off control method utilized in this equipment resulted in only 20% cycle operation time and a subsequent reduction of 20% in cycle COP relative to the cycle COP under steady state operation. It was determined that the transient performance of an absorption refrigeration cycle can be below the steady state performance, thereby reducing the actual observed COP in operation. Several common transient conditions that can occur include cycle start up, a varying evaporator load, or varying atmospheric conditions. This reduction in COP during transient conditions coupled with the fact that the transient performance of an absorption refrigeration cycle largely determines the energy efficiency during critical periods [12] suggests that improving the transient response of absorption refrigeration cycles via control will be beneficial. Additionally, many new applications for absorption refrigeration systems such as cooling a refrigerated trailer, space conditioning of an RV, or a man portable cooling unit will experience many more transient conditions than cycles operating in industrial plant conditions. Besides improving transient performance of ammonia refrigeration systems, active control can optimize the cycle COP. Jose Fernández-Seara in [13] describes how

variation in either the cycle's "external requirements" or the "external thermal conditions" leads to the cycle operating out of the design point, resulting in a suboptimal cycle COP. While the cycle is actuated by waste heat, Fernández-Seara contends that "design improvement and control optimization are crucial issues, regardless of the energy source being used."

2.5. Control Methods

Several recent research efforts have investigated the effect of different control strategies on absorption refrigeration cycle COP. Dence in [12] developed a transient model of an ammonia-water heat pump which was subsequently used to evaluate the response time of the system for different control schemes. In that work, the heat into the desorber was varied to control the cooled space temperature. Dence found that while a proportional-plus-derivative (PD) control loop improved the system's response time, it also resulted in increased overshoot. Investigations into an on-off generator control scheme also improved transient performance with only a 1% reduction in the cycles COP. Garimella in [14] created a model of a triple-effect absorption heat pump which was utilized to determine the effect of heat exchanger sizes and different control schemes on cycle performance. Two control strategies were investigated. The first was to maintain a constant high pressure loop desorber outlet temperature by varying the solution flow rate. The second strategy was to maintain a constant solution flow rate by allowing the desorber pressure and temperature in the high pressure loop to vary. Garimella found that the control strategies resulted in different cycle COP values for the same operating conditions.

For ambient temperatures above 95 °C the second control strategy, maintaining a constant solution flow rate, resulted in higher COP values.

The absorption refrigeration controls research most applicable to this study was performed by Jose Fernández-Seara in [13]. Fernández-Seara reports that "the generation temperature affects the ammonia absorption systems COP and that there is a temperature value called [the] optimal generation temperature (OGT) for which the [cycle] COP is maximum." Moreover, the OGT for a specific ammonia absorption refrigeration system (AARS) is only dependent on thermal operating conditions [13]. Since cycle COP is maximized when the heat of desorption Q_{des} is minimized, the OGT operating conditions are the same operating conditions as f^*_{opt} from [1]. Thus both observations by Mouchka and Fernández-Seara agree, that operating the desober at f^*_{opt} or the OGT (which is equivalent) results in an optimal cycle COP for the given cycle conditions.

Implementing the control strategy suggested in [13] to continuously maintain the generator at the OGT results in the absorption refrigeration system (ARS) performing at the maximum COP possible for the immediate thermal operating conditions. By continuously controlling the OGT the COP can be maximized as the external thermal conditions vary. The control strategy presented utilized on-off control of the refrigerant to the evaporator to control the "cooled space" temperature and PID control of the generator temperature, using heat as the controller input with the OGT as the reference temperature or set point. The control strategy proposed in

[13] was based on a parametric analysis of a simple model of an ARS. No simulation of the controlled closed-loop system was performed nor was any physical testing carried out. This work aims to both simulate the closed-loop response of the desorber to changes in the applied heat load and test a PID controller on an actual fractal-like branching desorber.

3. EXPERIMENTAL APPARATUS AND DATA ACQUISITION

An experimental apparatus for testing microscale, fractal-like branching microchannel desorbers was developed in the Microscale Transport Enhancement Laboratory at Oregon State University. This chapter explains the apparatus, its function and operation, as well as the data acquisition used to characterize desorber performance.

3.1. Existing Experimental Apparatus

The experimental apparatus was originally designed for testing desorption under steady state conditions. This study required operating under fluctuating conditions which required modifications to the setup. This section explains the existing equipment setup.

3.1.1. Fractal-like Branching Microchannel Desorber

Desorption is the process of generating vapor predominate in one substance from a liquid mixture of two or more substances [15]. In that regard it differs from evaporation which would have the same concentration of each substance in vapor form as it did in liquid form. The approximate fractal desorber used in this study can be viewed in a simplistic analysis as a heat exchanger as is shown in figure 3.1. Ammonia hydroxide flows through one side of the heat exchanger while hot heat transfer oil flows through the other. The heat transfer from the oil to the ammonia hydroxide is the mechanism responsible for the desorption process. Only part of the inlet stream is desorbed into ammonia rich vapor. The rest of the stream exits the desorber as liquid with a weak ammonia concentration.

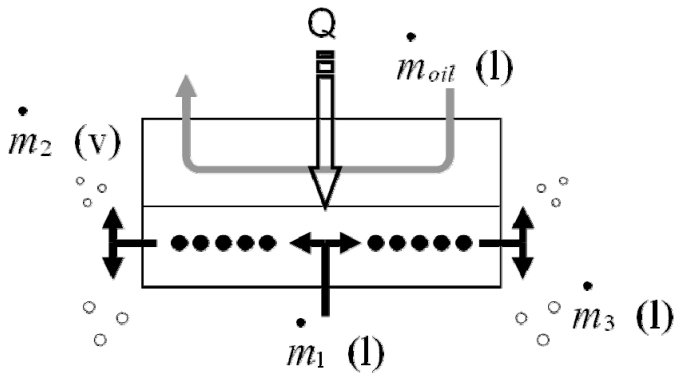

Figure 3.1: Schematic of an oil heated fractal-like branching microchannel desorber

Figure 3.2 below shows a detailed exploded view of the desorber used in this study, it is the same desorber design used by Mouchka in his work. The desorber consists of 5 stainless steel layers which, when diffusion bonded together, create the unit. Layers 3 & 5 have the fractal-like branching pattern etched onto one side, while layer 4 has the pattern etched onto both sides. Ammonia hydroxide flows in the microchannels created between layers 4 and 5. The hot oil flows between the channels created between layers 3 and 4. Layers 1 and 2 are added to create an annular plenum for the oil to be collected and to flow back out of the desorber as shown by the arrows in the figure. The ammonia hydroxide flows radially out of the desorber and is collected in the test manifold, which acts as a flash chamber.

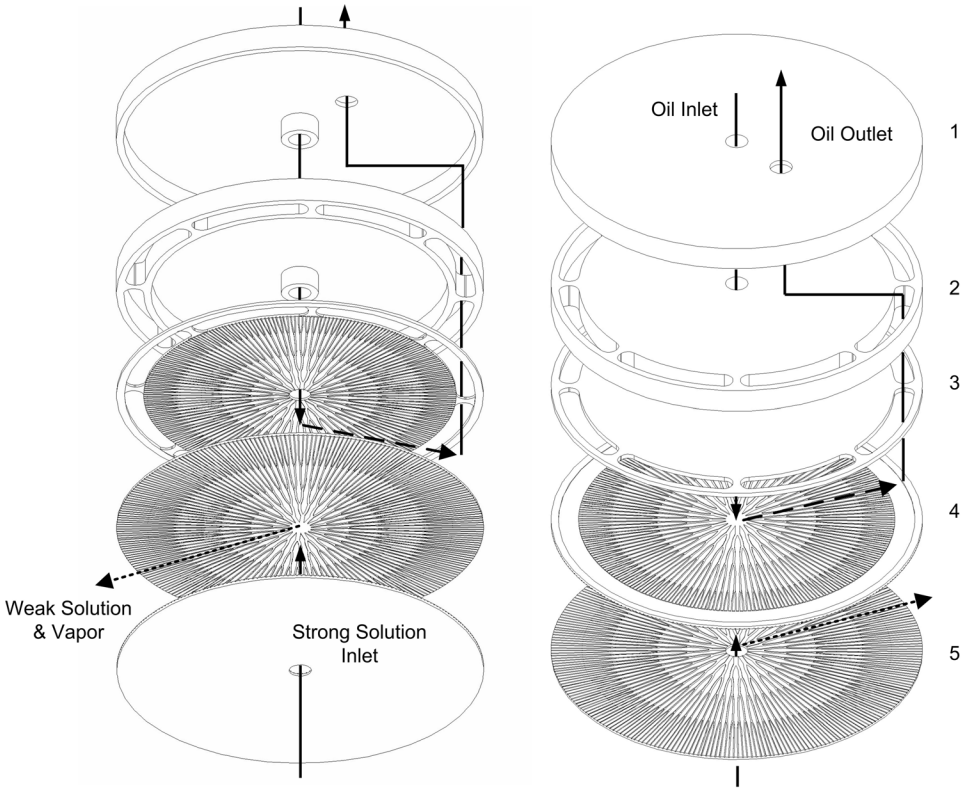

Figure 3.2: Exploded view of the desorber layers (used with permission, [1])

Detailed information about desorber manufacturing including information on channel geometry, materials used, channel etching, and layer bonding can be found in the thesis by Mouchka [1].

3.1.2. Test Manifold

The test manifold is considered part of the desorber because the ammonia hydroxide vapor and solution leaving the desorber disk must be collected and separated for useful desorption to occur. The test manifold performs this function while additionally serving as a mounting location for several crucial instruments. The ammonia hydroxide leaves the desorber disk as vapor and liquid. It then separates and collects in the test manifold with the solution weak in ammonia falling

to the bottom of the test manifold. The liquid in this volume of fluid is referred to as the holdup volume which was held as constant as possible throughout all tests. The ammonia rich vapor collects in the upper portion of the test manifold. In this way the test manifold acts as a gravity driven separator, see figure 3.3. It is important to note that the vapor and weak solution are in thermodynamic equilibrium at their interface.

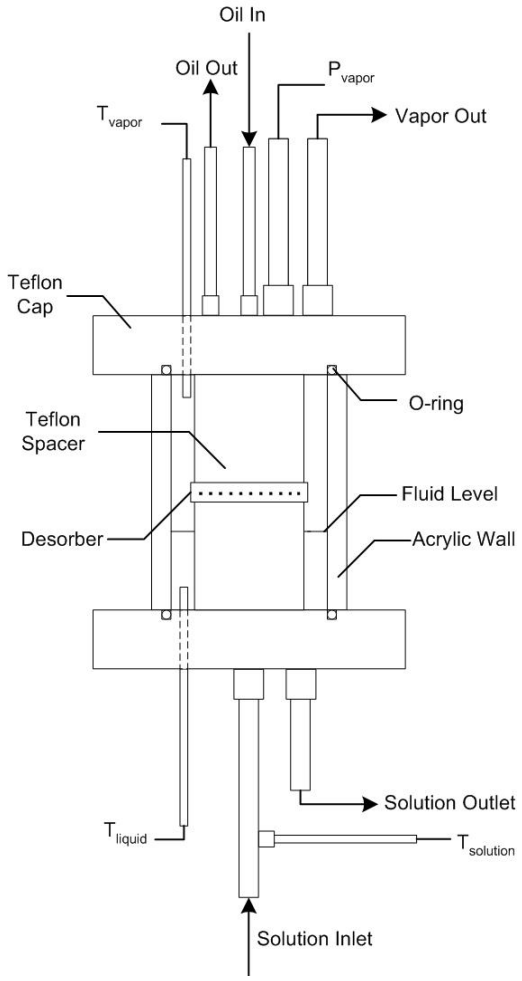

Figure 3.3: Test manifold schematic (used with permission, [1])

For additional information on the test manifold including design and instrumentation see Mouchka [1].

3.2. Flow Loop and Instrumentation

Figure 3.4 below shows the experimental flow loop used in this study. This is nearly the same loop that Mouchka used in his work with only one minor modification; the addition of a solenoid valve used for manifold pressure control during testing. The loop can be divided into two main parts: the oil sub-loop and the ammonia-water sub-loop.

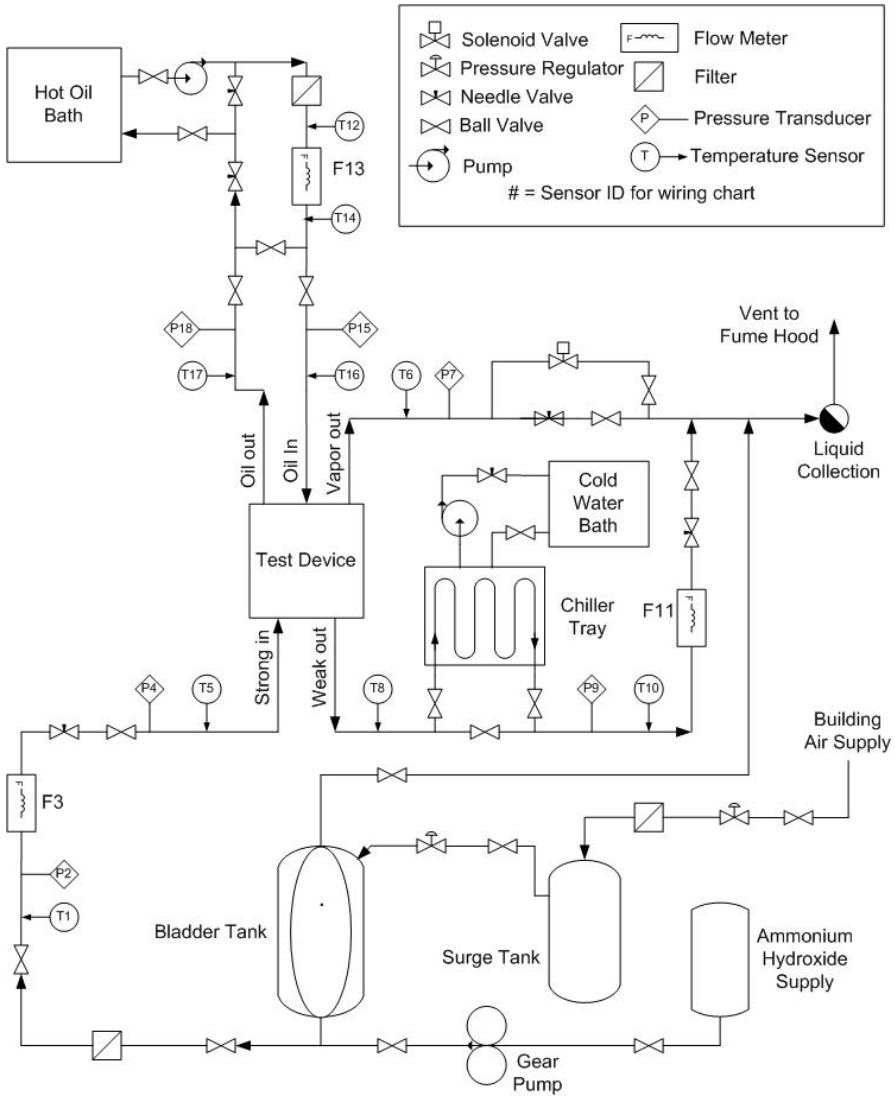

Figure 3.4: Experimental flow loop diagram

3.2.1. Oil Sub-Loop

An absorption refrigeration cycle becomes more attractive than other refrigeration cycles in situations where the cycle can be operated off of waste heat. Additionally the cycle performs the best when that waste heat is at a high temperature and can transfer heat with a small temperature drop between the oil inlet and outlet temperatures [16]. The oil sub-loop represents the waste heat source for the cycle. The amount of heat transferred to the ammonia hydroxide for desorption is dependent on many factors including oil temperature and oil flow rate. The oil sub-loop is designed to allow for the variation of either. The main components of the loop include a heater, pump and variable speed drive, and filter. Instrumentation includes a flow meter, pressure transducers, and temperature measuring thermocouples. The loop was designed to include a bypass loop to allow for filtering of the oil without flowing through the desorber should the oil become contaminated. Additional information on the oil loop including part numbers and additional explanations can be found in Appendix 1 and in [1], respectively. A new oil pump drive was purchased to allow for computer control of the oil flow rate by adjusting the pump speed. The drive receives a 2-10V proportional signal to set the pump speed. A power supply with a general purpose interface bus (GPIB) is used to allow the computer to set the voltage signal and thus the pump speed.

3.2.2. Ammonia-Water Sub Loop

A desorber is just one component of an absorption refrigeration cycle, the ammonia-water sub-loop in the experimental apparatus accomplishes the functions

of other cycle components. The strong solution, which would normally come to the desorber from the absorber in a full cycle, is supplied to the desorber from a pressurized bladder tank. The weak solution, which exits the test manifold and would flow back to the absorber in a complete cycle, is collected for disposal. The ammonia vapor which would be sent through the rectifier to the condenser, is disposed of as well. Key parts of the ammonia-water sub loop include the surge tank, bladder tank, filter and several valves. Instruments in the sub-loop include Coriolis mass flow meters also capable of reporting density, pressure transducers and thermocouples and resistance temperature detectors (RTD's). The strong solution flow rate into the desorber is controlled by the pressure difference between the bladder tank and the test manifold. A needle valve is used for setting the flow rate for a given pressure difference. Additional information on the instruments and equipment used in this loop can be found in Appendix 1 and in [1].

3.3. Solenoid Pressure Valve

A solenoid valve was installed on the existing flow loop and is used to automatically control the pressure in the test manifold via a computer control program. It replaces the needle valve that was used in earlier studies to accomplish the same purpose. Computer control was deemed necessary because the system identification tests will vary the oil flow rate significantly and rapidly and it would have been difficult to manually adjust the valve to maintain a constant pressure in the presence of these fluctuations.

3.3.1. Test Manifold Pressure

The pressure in the test manifold has a direct influence on the desorption process. Figure 3.5 shows the ammonia water $T - x$ diagrams for two pressures. Increasing the pressure shifts both the boiling and condensation lines upward. Thus for a given inlet solution concentration increasing the manifold pressure increases the temperature at which desorption begins, the saturation temperature (T_{sat}). This in turn changes the heat of desorption required for a given strong solution flow rate.

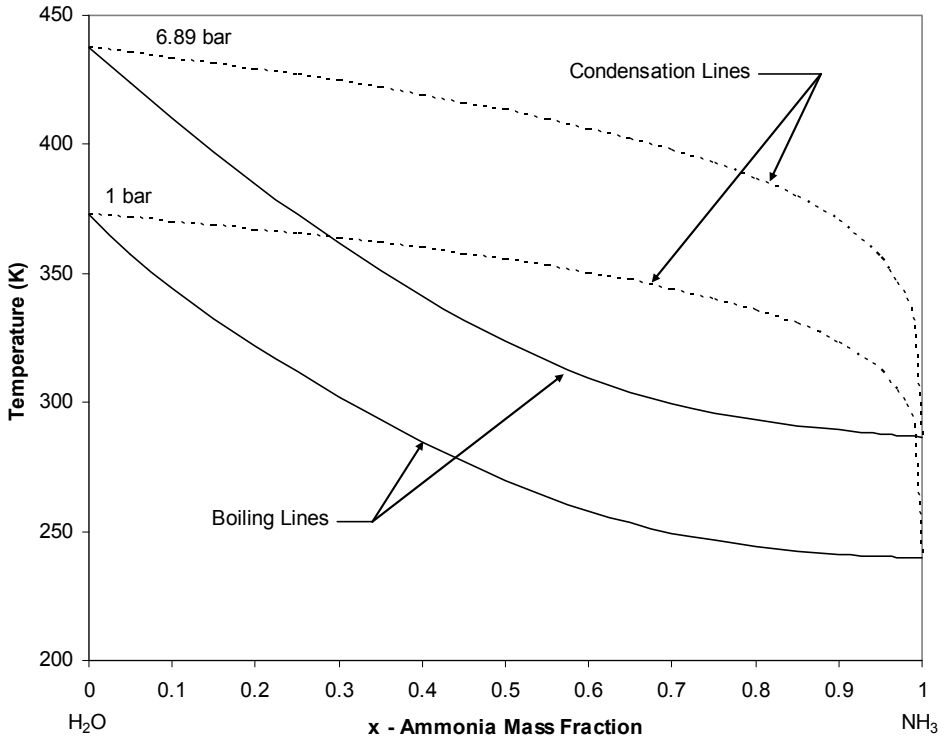

Figure 3.5: $T - x$ diagrams for various pressures

An additional pressure affect comes from the fact that the strong solution flow into the desorber is pressure driven. As the manifold pressure changes, the strong solution flow rate changes as well, this changes the amount and quality of vapor

produced. It was important to minimize these affects during testing by maintaining a constant manifold pressure. The existing setup was designed for steady state operation which only required a needle valve for controlling the exiting vapor stream flow rate and thus the manifold pressure. This method was not sufficiently robust for the current testing. A new approach for controlling the pressure was therefore implemented.

3.3.2. Valve Setup

The replacement solenoid valve was chosen to match the needle valve properties as closely as possible. The solenoid valve is an “on/off” valve meaning that it is closed when no voltage is applied and open when a voltage is applied. The application requires a valve that can be gradually closed. This was accomplished with valve control electronics available for solenoid valves. The circuit creates a pulse width modulation (PWM) signal that allows the “on/off” valve to be opened gradually. The solenoid valve was installed in the flow loop in parallel to the needle valve as figure 3.4 illustrates. This was done to allow for other laboratory tests to be conducted using the needle valve. Ball valves were installed near each valve to allow for easy switching between the two valves. The valve control electronics are equipped with three resistors which control the solenoid coil current and directly affect the valve performance. These resistors must be calibrated for the specific application. The description of the calibration procedure in the operating instructions assumes that the valve will control the fluid flow rate at a relatively constant pressure drop

across the valve. In the intended application the valve will control the pressure by varying the vapor flow rate. The procedure followed to set the resistor values is described in Appendix 2.

3.3.3. PID Valve Control

A PID controller was used for the pressure control because of its simple form and relatively easy implementation. The standard form of PID controller equation (2) comes from the Laplace domain and cannot be directly applied to a discrete time domain application, as is needed for the valve control. Keen [16] shows that the PID controller takes the following form for a discrete time domain application:

$$u(t) = u(t-1) + K_p[e(t) - e(t-1)] + K_i T_s e(t) + \frac{K_d}{T_s}[SV(t) + SV(t-2) - 2SV(t-1)], \quad (5)$$

where SV is the plant variable; in this case the manifold pressure (P_{man}). Equation (5) was implemented in National Instruments software LabVIEW™ as part of the preexisting data acquisition program. There are several common PID tuning rules in the literature. The PID controller was tuned using rules suggested by Skogestad in [17]. A 1st order approximation of the dynamics was found from a plot of the pressure responding to a step change in the valve control voltage. From this approximation model PI gains were found. The controller had difficulty reacting to the sudden pressure changes that accompanied step changes in oil flow rate. To

compensate, both ball valves were open during testing and the manual pressure valve was used in conjunction with the solenoid valve to regulate the pressure.

3.4. System Identification Test Plan

The purpose of this research is to design and implement a controller that regulates f^* to desired values by varying the oil flow rate ($\dot{m}_{oil}$). The reasoning for choosing f^* and $\dot{m}_{oil}$ as the controlled variable and controller input respectively is explained in 4.1 and 4.2. The design of any controller requires a model of the system to be controlled. Since a model of the desorber could not be derived from first principles, system identification techniques were used to determine a model for controller design.

This study also investigates the robustness of the controller to oil temperature strong solution flow rate and pressure changes. To do so, four different operating conditions for model generation were chosen based on the work done by Mouchka [1]. The testing conditions chosen are represented in table 3.1 as letters.

Table 3.1: System identification test points
($P_{manifold}$ = 20 psi)

		Oil Temperature (°C)	
		100	120
Strong Solution Flow Rate (g/min)	25	D	C
	35	E	A, B

The purpose of multiple operating conditions was to determine whether a single model could be applied to varying operating conditions, within the specified range,

or if different models were needed as oil temperature or strong solution flow rate change. Letter B is a repeat test of the operating conditions of test A.

3.5. Data Acquisition

Data was gathered using LabVIEW™ software in conjunction with corresponding National Instruments data acquisition hardware. See Appendix 1 for the hardware listing. Desorber parameters including pressures, temperatures, flow rates, and densities, were monitored throughout each test. Specifically, the data from each instrument in fig. 3.4 was recorded. A data point was collected roughly every 6 seconds. Each data point consisted of many repetitions which were averaged together. Thus each data point consisted of an average repetition value with an associated standard deviation. Appendix 3 contains a table listing the relevant instrumentation and the repetitions of that sensor for each data point. Additionally Mouchka [1] provides a thorough explanation of the data acquisition setup.

3.6. Operating Procedures

The operating procedure used in earlier testing required updating for the additional equipment added to the flow loop. The same procedure was used for each system identification test to ensure safety and uniformity in the data collected. The detailed operating procedure is included in Appendix 4 and a brief summary follows.

The oil is heated in the oil bath during a warm up period. During this time the oil pump is turned on using the GPIB power supply, and the oil is circulated in the manifold bypass loop. Once the oil is brought to temperature, strong solution flow is started and a holdup volume is established in the test manifold. With the holdup

volume sufficiently large the oil loop valves are adjusted to begin the oil flow through the desorber. As vapor production begins, increasing the pressure in the test manifold, the flow of the weak solution stream begins allowing for the initiation of the data acquisition program. From this point on the desorber is brought to steady state operating conditions by adjusting the oil flow rate, manifold pressure, and strong and weak solution flow rates. Once steady state conditions have been established for approximately 5 minutes the system identification test is begun.

At the conclusion of the test after finishing data acquisition the oil valves are closed to stop the oil flow through the desorber, and the strong solution ammonia flow is reduced. Once the temperature of the desorber has cooled the strong solution flow is stopped, and the desorber is rinsed with pure deionized water to reduce any corrosion effects.

4. SYSTEM IDENTIFICATION AND DATA ANALYSIS

A system identification test was designed and implemented for mathematical model generation of the dynamic response of the rectified circulation ratio to oil mass flow rate changes in the desorber. Liquid concentrations were calculated using a Gibbs free energy approach. Uncertainties in instrumentation measurements and error propagation were quantified. The system identification was performed using MATLAB® System Identification Toolbox and 2nd order process models were selected for simulation.

4.1. System Identification Test Design

System identification produces a model of the system dynamics that govern the relationship between input and output variables that cannot be derived from first principles. The system identification test enables the creation of a linear model relating the variables of interest, as determined by the test design.

4.1.1. Desorber and Desorber/Rectifier Mass Balances

Examination of the mass balances of a desorber and a desorber/rectifier system provides insight into the appropriate selections of the system input u(t) and output y(t). As illustrated in the desorber schematic or Fig. 3.1, reproduced below, the different streams of ammonia-water entering and leaving the desorber are uniquely identified by the following notation.

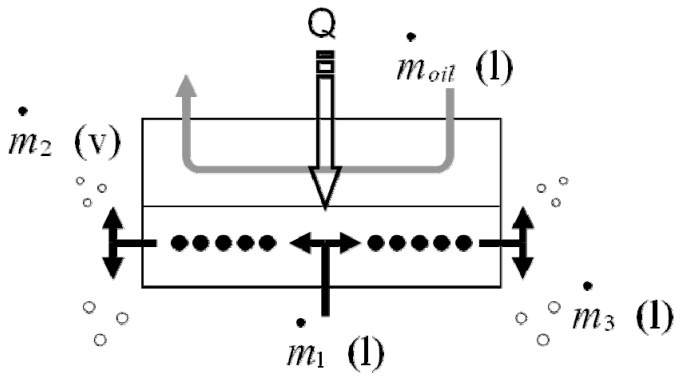

Figure 3.1: Schematic of an oil heated fractal-like branching microchannel desorber

Stream 1 represents the desorber inlet stream, which is a liquid stream concentrated in ammonia and hereafter is referred to as the "strong solution" stream. Stream 2 represents ammonia rich vapor stream leaving the desorber and hereafter is referred to as the "vapor" stream. Stream 3 represents the exiting liquid stream, which is weakly concentrated ammonia. It is hereafter referred to as the "weak solution" stream.

A mass balance of the desorber can be written

$$\dot{m}_1 = \dot{m}_2 + \dot{m}_3 \tag{6}$$

or in terms of an ammonia mass balance

$$x_1 \dot{m}_1 = x_2 \dot{m}_2 + x_3 \dot{m}_3 \tag{7}$$

with x, the ammonia concentration, defined as

$$x = \frac{\dot{m}_{NH_3}}{\dot{m}_{H_2O} + \dot{m}_{NH_3}}. \tag{8}$$

It is common to define the circulation ratio (f) as

$$f = \frac{\dot{m}_1}{\dot{m}_2}. \tag{9}$$

The inverse of the circulation ratio is called the dryness fraction (d_f) which represents the mass flow rate of vapor produced per unit mass flow rate of strong solution into the desorber

$$d_f = \frac{1}{f} = \frac{\dot{m}_2}{\dot{m}_1}. \tag{10}$$

Combining equations (6, 7, & 9) the circulation ratio can be expressed in terms of the ammonia concentrations

$$f = \frac{x_2 - x_3}{x_1 - x_3}. \tag{11}$$

While the desorber has a direct influence of the cycle COP, it is not the cycle and insights are gained from examining a control volume of the desorber and rectifier. This is especially the case for a co-flow desorber, such as the one used in this study, which relies heavily on rectification to reach a sufficiently high refrigerant vapor concentration. Following the same process on a control volume that contains both the desorber and rectifier first requires an ammonia mass balance. It is subsequently necessary to assume that the reflux out of the rectifier is approximately equal to the weak solution leaving the desorber. The assumption is reasonable, as explained below, and results in the following equation for the desorber/rectifier system circulation ratio or rectified circulation ratio

$$f^* = \frac{x_{2^*} - x_3}{x_1 - x_3}, \tag{12}$$

where x_{2^*} is the ammonia concentration of the vapor stream leaving the rectifier. In practical applications water remaining in the ammonia vapor stream will result in a temperature glide of the refrigeration cycle resulting in an undesirable drift of the operating conditions of the cycle. Because of this, x_{2^*} is typically chosen to be 0.99 or higher and was fixed at 0.99 for this study yielding

$$f^* = \frac{0.99 - x_3}{x_1 - x_3}. \tag{13}$$

A detailed explanation of the derivation of equation (13) is included in Appendix 5. The rectifier reflux assumption is reasonable because the amount of reflux is sufficiently small to not change significantly conditions in the desorber. The assumption allows for f* to be dependent on only desorber states except for the rectified vapor stream concentration, which is usually prescribed by the refrigeration cycle design. Thus f* can be calculated based solely on the concentrations of strong and weak solution streams of the desorber. With both f and f* defined the description of the system input and output selection can proceed.

4.1.2. System Input and Output

Single-input single-output (SISO) systems represent the simplest models of system dynamics, yet controllers designed for such systems are often surprisingly robust. Modeling the desorber dynamics as a SISO system requires the selection of a single input and output from the model parameters to generate a SISO model.

Mouchka investigated the affect of oil mass flow rate, oil temperature, and inlet solution flow rate on vapor mass flow rate and vapor mass fraction [1]. Of the three parameters investigated oil mass flow rate presented the best choice for the controller input $u(t)$. Strong solution flow rate into the desorber in an actual absorption refrigeration cycle is not easily adjustable. In fact, the flow rate is determined by the capabilities of the absorber and in practice the entire cycle is designed for a set strong solution flow rate into the desorber. Oil temperature is not readily varied because of the large thermal mass involved and is therefore impractical. However, oil flow rate is easily varied by using a variable speed pump or a proportional control valve. Additionally, Mouchka determined in [1] that vapor mass flow rate, vapor mass fraction, and circulation ratios were all dependent on oil flow rate. The oil mass flow rate has a direct influence on desorber temperature, heat transferred to the ammonia water, and thus the amount and quality of ammonia vapor generated. The oil mass flow rate is directly measurable from flow meter 13 (see figure 3.4) and is proportional to the pump drive voltage signal. These characteristics of the experimental setup enable easy control of the oil mass flow rate. For these reasons, oil mass flow rate was chosen as the SISO system input $u(t)$.

As discussed in Chapter 1, several possible choices exist for the controlled variable, $y(t)$. Vapor concentration, x_2, vapor mass flow rate, $\dot{m}_2$, circulation ratio, f, and rectified circulation ratio, f^*, were initial candidates. The goal of the controlled variable selection was to choose a single variable that, when controlled,

would maximize both the vapor concentration and vapor flow rate. While control of multiple variables might be utilized to achieve this goal, a single variable was sought to preserve the SISO model of the system. A natural trade-off exists in the desorption process between x_2 and $\dot{m}_2$. Addition of heat to the strong solution stream generates more vapor, and as the vapor generation increases the amount of water in the vapor also increases. This results in a decrease in ammonia mass fraction, or concentration, in the vapor stream. The interaction between vapor concentration and vapor flow rate precludes the use of either as the controlled variable. For example, maximizing vapor concentration would result in minimizing the vapor flow rate, thereby making the control impractical. In a similar manner, controlling vapor flow rate would also be impractical since it would minimize the vapor mass fraction.

As discussed in Chapter 1, desorbers must generate ammonia vapor with some water content due to the similar vapor pressures of water and ammonia [18]. A rectifier is, therefore, required to purify the vapor stream leaving the desorber in order to prevent water collection in the evaporator and temperature glide [1]. This is especially true of co-flow desorbers. As was discussed in chapter 2, Mouchka determined that the minimum heat of desorption for a desorber/rectifier system occurs at a value called the optimal rectified circulation ratio f^*_{opt}. The f^*_{opt} also corresponds to the OGT as described in Chapter 2. When a desorber/rectifier system is operated such that f^* is above f^*_{opt} the desorber is run below the OGT with little boiling, resulting in a high vapor ammonia concentration but low vapor mass flow

rate. Operating in this regime requires a larger desorber to meet cycle requirements. Conversely when the desorber/rectifier system is operated such that f^* is below f^*_{opt} the desorber is run above the OGT with abundant boiling, yielding a higher vapor mass flow rate, but at a lower vapor ammonia concentration. Operating in this regime increases the required rectification. Mouchka in [1] provides an excellent graphical depiction of this trade-off, without the explanation of f^* in relation to f^*_{opt}. Selecting the rectified circulation ratio f^* as the controlled variable incorporates this natural trade-off. Thus it made an excellent choice for the controlled variable. With the SISO input and output identified, additional data was collected through preliminary testing to design the identification test signal.

4.1.3. Preliminary Process Tests

Constructing an appropriate identification test signal requires knowledge of the system response. At a minimum the approximate process or settling time of the controlled variable y(t) is required. Imparting a step change in the oil mass flow rate yielded the response plot of f^* illustrated figure 4.1. The settling time of the f^* can be found from the plot. It is the time, after the step change of the input, for the controlled variable to reach and stay within ± 2% of its steady state value.

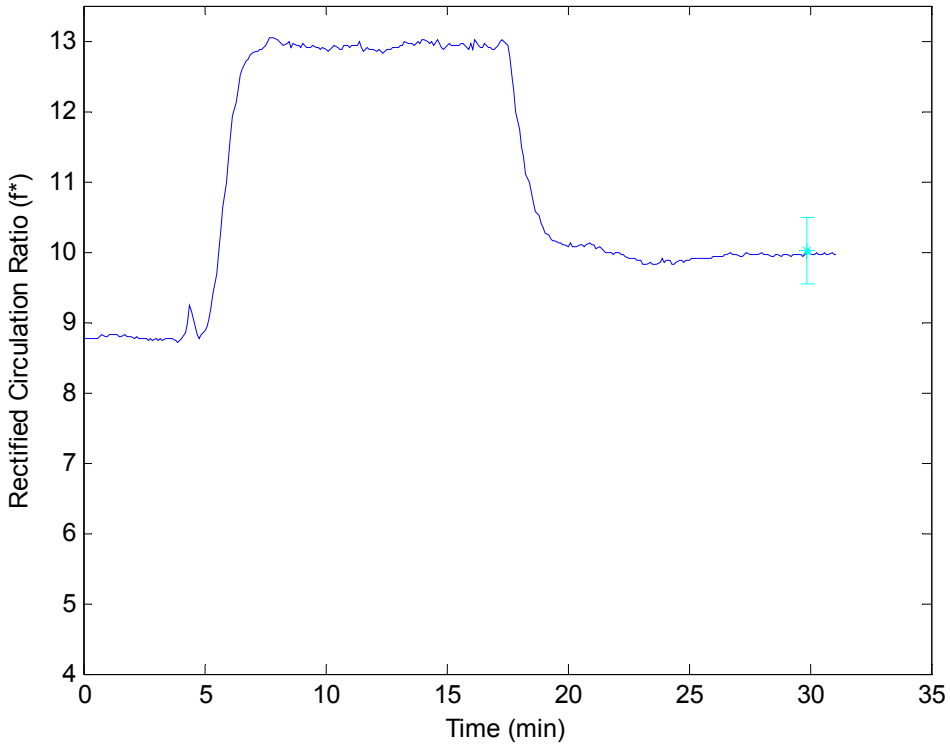

Figure 4.1: Rectified circulation ratio step response to various oil flow rate step inputs

From figure 4.1 the settling time of f* was estimated to be approximately 360 seconds.

4.1.4. Identification Test Signal

With the settling time established, the identification test was designed according to the recommendations of [19]. An open loop test was implemented having a duration 18 times the settling time or approximately 108 minutes. The test signal shape was constructed in accordance with the guidelines as general binary noise, with the oil pump control voltage switching between 5.25 and 8.75 volts. These voltages correspond to nominal oil flow rates of 245 and 530 g/min, respectively. The amplitude of the signal was chosen to be as large as possible to give a good

signal to noise ratio in the test while staying within flow rates reasonable for the desorber. The mean switching time for the test was determined based on the recommended design rule in [19] of

$$ET_{sw} = \frac{Ts_{98\%}}{3} \tag{14}$$

where ET_{sw} is the mean switching time of the signal, and $Ts_{98\%}$ is 98% of the settling time of the system. Because the switching of the signal was random, none of the identification test signals were the same. Figure 4.2 below shows the test signal for test A, which is representative of all the identification test signals used.

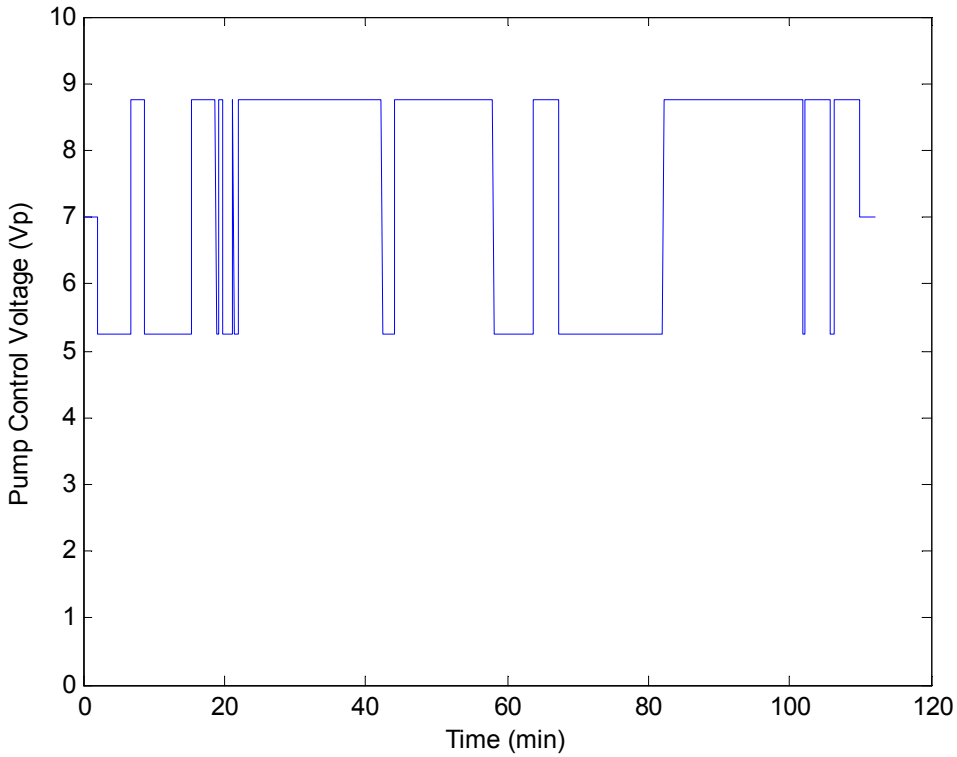

Figure 4.2: The identification test signal for test A

The smallest process time constant that is detectable from the identification test is based on the sampling rate of the data acquisition system. A reasonable estimation of this time is

$$\tau_{\min} = 3T \tag{15}$$

where $\tau_{\min}$ is the smallest process time constant identifiable and T is the sampling rate. The sampling rate for the data acquisition system was 6 seconds, yielding a minimum identifiable process time of 18 seconds. As a result, if the relationship between f^* and $\dot{m}_{oil}$ had a process time constant faster than 18 seconds it would not be identifiable with the existing experimental setup. Experience with the desorber from initial testing indicated the process time was much slower.

4.1.5. Identification Testing

The identification testing procedure used followed the operating procedures outlined in Chapter 3 to bring the system to steady state. After attaining steady state for a minimum of 5 minutes, the identification test was started. During the test the pump voltage and manifold pressure were controlled by the computer. The operator was only required to vary the weak stream solution flow rate to maintain a constant holdup volume in the test manifold and assist with the pressure regulation during the oil flow rate step changes. The tests specified in table 3.1 were carried out over a period of two days, after which the testing results were analyzed and the identification carried out as detailed in the following sections.

4.2. Data Analysis

4.2.1. Liquid Concentrations

As illustrated in equation (13), the controlled variable f^* depends only on the strong and weak solution ammonia concentrations of the desorber. Therefore, accurate measurements of the liquid concentrations were critical to this study. While the concentration / mass fraction of the liquid streams cannot be measured directly; as a binary mixture of ammonia and water, the state of the liquid can be calculated from three independent intensive properties. The three properties used in this study to calculate the mass faction were pressure, specific volume and temperature, with specific volume calculated from the measured density. All three measurements were obtained within a short span of tubing in the experimental test loop. The mass fraction of the strong solution was found from

$$x_1 = \varphi(T_1, P_2, v_3)\,, \tag{16}$$

while the weak solution mass fraction was determined from

$$x_3 = \varphi(T_{10}, P_9, v_{11})\,. \tag{17}$$

See figure 3.4 for the locations of each instrument in the flow loop.

4.2.2. EES Calculation Method

The pressure, temperature, and specific volume measurements were used to calculate the mass fraction from known equation of state correlations. The software Engineering Equation Solver (EES) is equipped with an additional library called NH3H2O which includes the equation of state correlations from [20]. This library,

combined with the features of EES, provides a quick and reliable method for calculating solution mass fractions through an iterative scheme. The EES code used for the mass fraction calculation, "awx_proc" is included in Appendix 6, and is the same used by Mouchka in [1]. Controller implementation required calculation of the controlled variable f^* in each iteration of the DAQ routine. Since the EES software cannot currently be run from within LabVIEW™ another method for calculating the liquid concentrations was required, and is described in the following section.

4.2.3. MATLAB Calculation Method

As suggested by El-Shaarawi in [21], a Newton Raphson method was used along with the Gibbs excess energy function proposed by Ibrahim in [20] to calculate the liquid mass fraction from pressure, temperature, and specific volume. Ibrahim [20] provides an expression for the molar volume of the liquid mixture as

$$v_m^L = y v_a^L + (1-y) v_w^L + v^E, \tag{18}$$

where y is the ammonia mole fraction, v is the molar volume, and each term in the above equation is nondimensional. v^E is the excess volume for the liquid mixture, subscript m denotes mixture, a ammonia, and w water, superscript L represents liquid phase. The excess molar volume of the liquid is related to the excess Gibbs free energy by

$$v^E = \frac{RT_B}{P_B}\left[\frac{\partial G_r^E}{\partial P_r}\right]_{T,y}, \tag{19}$$

where R is the gas constant, T_B and P_B equal 100 K and 10 bar respectively, G_r^E is the Gibbs excess energy for liquid mixtures and P_r is pressure nondimensionalized by P_B. The partial derivative with respect to nondimensionalized pressure of the correlation representing G_r^E, determined by Ibrahim, was taken. The resulting equation relating mole fraction and molar volume was used along with the Newton Rhapson method to iterate from an initial guess to the correct mass fraction of the liquid. Appendix 7 includes the equation derivation as well as the MATLAB code utilized within LabVIEW™ for the calculation.

The code was validated for a variety of testing conditions by comparing the MATLAB calculated concentration values with those found using EES for the same pressure, temperature, and density. Good agreement was obtained between both methods, with the MATLAB calculations of the concentrations yielding an average percent error of 1.83%. Calculation of the liquid concentrations, and thus f^*, via this routine enabled an accurate f^* calculation for each iteration of the DAQ routine. As a result, the f^* value could then be used as the controlled variable signal for control system design.

4.3. Uncertainty

Precision, bias, and propagation errors in the measured data are explained and quantified below.

4.3.1. Precision Error

The precision error in any independent variable is a measure of the repeatability of the measurement system and the variation in the measurements taken. The precision error for measured values is quantified in this study as

$$u_p = t_{N,95\%}(S_x) \tag{20}$$

where t is the Student t distribution for 95% confidence and N is the number of samples taken at each point; S_x is the pooled standard deviation of the means.

4.3.2. Biased Error

Biased errors are estimated in this study as the calibration errors of the instruments used. Many of the instruments were calibrated from earlier work and the biased errors are reported in Appendix 3 along with calibration equations and instrument uncertainties. Several new pressure transducers were installed in the flow loop and their biased errors were calculated as

$$u_B = \sqrt{(e_{s\tan dard})^2 + (e_{curvefit})^2} \tag{21}$$

where $e_{s\tan dard}$ is the error associated with the calibration standard used. $e_{curvefit}$ is the error of the curve fit and is

$$e_{curvefit} = t_{\upsilon,95\%} e_{std} \tag{22}$$

where υ is the number of degrees of freedom in the curve fit, $\upsilon = n - 2$, with n the number of data points taken and e_{std} defined as

$$e_{std} = \sqrt{\frac{\sum_{i=1}^{n}(y_i - y_{ci})^2}{\upsilon}} \tag{23}$$

where $y_i - y_{ci}$ is the difference between the measured, y_i, and predicted, y_{ci}, data.

4.3.3. Propagation error

Propagation error represents the uncertainty in calculated values based on the uncertainty in independent directly measurable variables. As described earlier, liquid ammonia concentration is a function of temperature, pressure, and density according to

$$x_i = \varphi(T_i, P_i, v_i)\,. \tag{24}$$

The sequential perturbation method described in [22] was used to calculate the propagation of uncertainty for liquid concentrations. The uncertainty is equal to

$$u_{x_i} = \pm\sqrt{\sum_{j=1}^{3}\left(\delta R_{ij}\right)^2} \tag{25}$$

where δR_{ij} is an approximation of the uncertainty contribution from each variable as determined by

$$\delta R_{i1} = \frac{\left|f(T_i + u_{T_i}, P_i, \upsilon_i) - R_0\right| + \left|f(T_i - u_{T_i}, P_i, \upsilon_i) - R_0\right|}{2}. \tag{26}$$

$$\delta R_{i2} = \frac{\left|f(T_i, P_i + u_{P_i}, \upsilon_i) - R_0\right| + \left|f(T_i, P_i - u_{P_i}, \upsilon_i) - R_0\right|}{2}. \tag{27}$$

$$\delta R_{i3} = \frac{\left|f(T_i, P_i, \upsilon_i + u_{\upsilon_i}) - R_0\right| + \left|f(T_i, P_i, \upsilon_i - u_{\upsilon_i}) - R_0\right|}{2}. \tag{28}$$

Uncertainty propagation affecting the rectified circulation ratio

$$f^* = \frac{0.99 - x_3}{x_1 - x_3}, \tag{29}$$

was found using the Kline-McClintock method [11]. The uncertainty of the rectified circulation ratio f^*, denoted as u_{f^*} is determined as

$$u_{f^*} = \pm\sqrt{\sum_{i=1}^{3}\left(\frac{\partial f^*}{\partial x_i}u_{xi}\right)^2}, \tag{30}$$

where the uncertainties u_{x_1} and u_{x_3} were found by the sequential perturbation method.

4.4. System Identification

Because a relationship between oil flow rate and rectified circulation ratio could not be derived from first principles, system identification techniques were used to experimentally identify the underlying dynamical relationship. The identification process was greatly simplified using the numerical routines provided by the computer software MATLAB®.

4.4.1. MATLAB® System Identification Toolbox

The input and output data from the system identification tests were processed utilizing MATLAB's System Identification Toolbox. The System Identification Toolbox is a set of numerical routines that provide a linear mathematical model from input and output data of a dynamic system. The resulting model, once validated, can subsequently be used in controller design as a substitute for the actual experimental system. The toolbox greatly simplifies the creation of such linear models by embedding the model estimation mathematics into MATLAB functions available in

a graphical interface. The System Identification Toolbox provides multiple methods for producing mathematical models from the input/output data provided. The models available include parametric, process, spectral, and correlation models.

4.4.2. Toolbox Process Models

Of the available model types, process models were selected to model the system dynamics for several reasons. First, process models lend themselves to SISO systems, such as that studied here, since they represent the system dynamics by a transfer function. Additionally, controller design for the model types which result from process models is relatively mature. Table 3.1, reproduced below for the readers convenience, shows the testing plan used for the five identification tests.

Table 3.1: System Identification Test Points
($P_{manifold}$ = 20 psi)

		Oil Temperature (°C)	
		100	120
Strong Solution Flow Rate (g/min)	25	E	C
	35	D	A, B

Each letter in the table represents an identification test of 1079 samples lasting approximately 108 minutes. Creation of a process model requires two data sets, one for system identification and the second for model validation. Model validation utilizes the system model and input data and compares the predicted output of the model to that obtained experimentally. Models that represent the underlying system dynamics well are capable of reproducing better fits to the experimental output data. Thus both data sets, one used for identification and the other for validation, produced a single mathematical model of the underlying dynamics under investigation. Table

4.1 below illustrates how the data from the five tests were used to generate six models representative of the dynamical relationship between f^* and $\dot{m}_{oil}$.

Table 4.1: Test Data Used for Model Generation

Test Name	Model Name	Oil Temp	Flow Rate	Samples in Test	Identification Data Points	Validation Data Points
A	A	120	35	1079	1 - 540	541 - 1079
B	B	120	35	1079	1 - 540	541 - 1079
-	AB	120	35	NA	1079 (A)	1079 (B)
C	C	120	25	1079	1 - 540	541 - 1079
D	D	100	35	1079	1 - 540	541 - 1079
E	E	100	25	1079	1 - 540	541 - 1079

The table shows that the data for models A, B, C, D, & E were segmented with the first half of the respective test data used for model identification and the second half used for the validation. Model AB was created differently, with the data for both identification and validation each being a complete test, tests A and B, respectively.

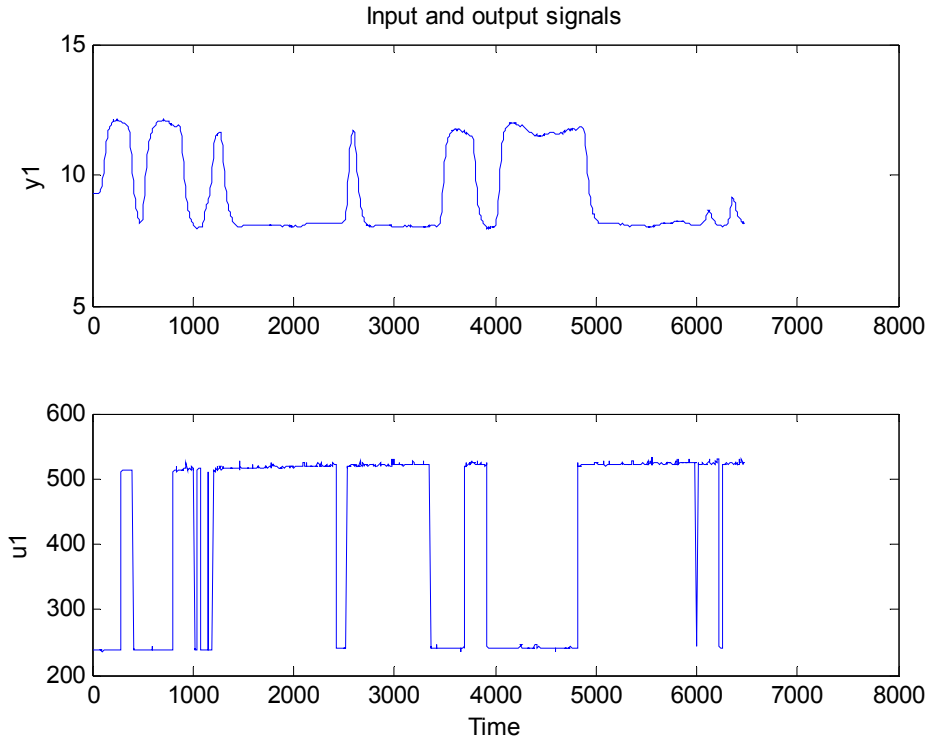

Figure 4.3: Input and output signals from identification test A

Figure 4.3 illustrates both y(t), f*, and u(t), the oil pump control voltage for system identification test A. A relationship between y(t) and u(t) is observable from fig. 4.3 as is a delay in the output after a change in u(t).

4.4.3. Transfer Function Selection

Use of the toolbox enabled calculation of forty-two different process models, resulting in an exhaustive search method for identifying models which best fit the testing data. Each of the forty-two models is a transfer function comprised of a combination of one, two, or three poles (real or complex), and a combination of a zero, delay, and/or integrator. The forty-two different process models were calculated for test A. The fit of these models ranged from 14.7% to 90.05% and are

included in Appendix 8. From these results the following five transfer functions were identified as the best candidates for an appropriate representation of the relationship between rectified circulation ratio and pump voltage.

$$P1D = \frac{ke^{-\theta s}}{(1+\tau_1 s)} \tag{31}$$

$$P2D = \frac{ke^{-\theta s}}{(1+\tau_1 s)(1+\tau_2 s)} \tag{32}$$

$$P2DIZU = \frac{k(1+T_z s)e^{-\theta s}}{s(1+(2\zeta T_w)s+(T_w s)^2)} \tag{33}$$

$$P3DZ = \frac{k(1+T_z s)e^{-\theta s}}{(1+\tau_1 s)(1+\tau_2 s)(1+\tau_3 s)} \tag{34}$$

$$P3DZU = \frac{k(1+T_z s)e^{-\theta s}}{(1+(2\zeta T_w)s+(T_w s)^2)(1+\tau_3 s)} \tag{35}$$

In the abbreviations PX, X is the number of poles in the model; D, I, or Z indicate a delay, integrator, or zero in the model; and U, if present, indicates complex poles. It should be noted that regardless of order, each of the candidate transfer functions has a time delay term $e^{-\theta s}$. This delay in the system limits the closed loop response achievable with a controller. The delay is a result of the experimental setup instrumentation requirements and comes from the time for the weak solution stream to travel from the desorber test manifold to instruments $P9$, $T10$, and $\rho 11$ in fig. 3.4. If it were possible to measure the weak solution stream temperature, density, and pressure at the desorber the delay would be eliminated. The distinction should be clear that the delay is part of the experimental setup desorber dynamics and not that

of the desorption process itself. The results of the different type of modeling fits for each transfer function are listed below in table 4.2.

Table 4.2: Percent fits of the various transfer functions for each model

	A	B	AB	C	D	E
P1D	86.35	85.79	83.64	86.13	82.92	87.97
P2D	87.55	85.78	85.49	87.63	84.55	89.01
P2DIZU	90.05	87.52	84.71	89.32	86.41	92.12
P3DZ	89.12	87.57	85.9	87.91	84.15	89.43
P3DZU	88.98	87.54	85.56	88.11	83.91	89.79

The fit is expressed as a percentage of the validation data predicted by the model. It can be seen from the table that the transfer function P2DIZU (2 complex poles with a delay integrator and zero) is the best fit for models A, C, D and E. While P2DIZU is the transfer function with the best fit, only small differences in fit exist for less complex transfer functions. For example the differences in fit between P2DIZU and P2D was only an average reduction of 2.1% for the six models. The difference in fit between P2DIZU and the simplest model, P1D (single real pole with delay) is only an average reduction of 3.5% for each of the six models. Because there was relatively little reduction in the transfer function fit with a substantial reduction in transfer function complexity, the P2D transfer function was chosen for modeling the dynamic relationship between rectified circulation ratio and oil flow rate for the desorber for each model. The 1st order transfer function P1D was included in initial testing as well.

4.5. Model Simulation

With the desired representation identified, the models were coded in MATLAB to enable simulation of the closed loop system response for various controller designs. Because system delay of the transfer function could not be simulated exactly, a seventh order padé approximation of the delay was utilized. Once each model was created in MATLAB, validation consisted of simulating the system response to a measured input, and comparing that with the actual measured response. Figure 4.4 below illustrates the simulated and measured response for model A, which is representative of the results for each model.

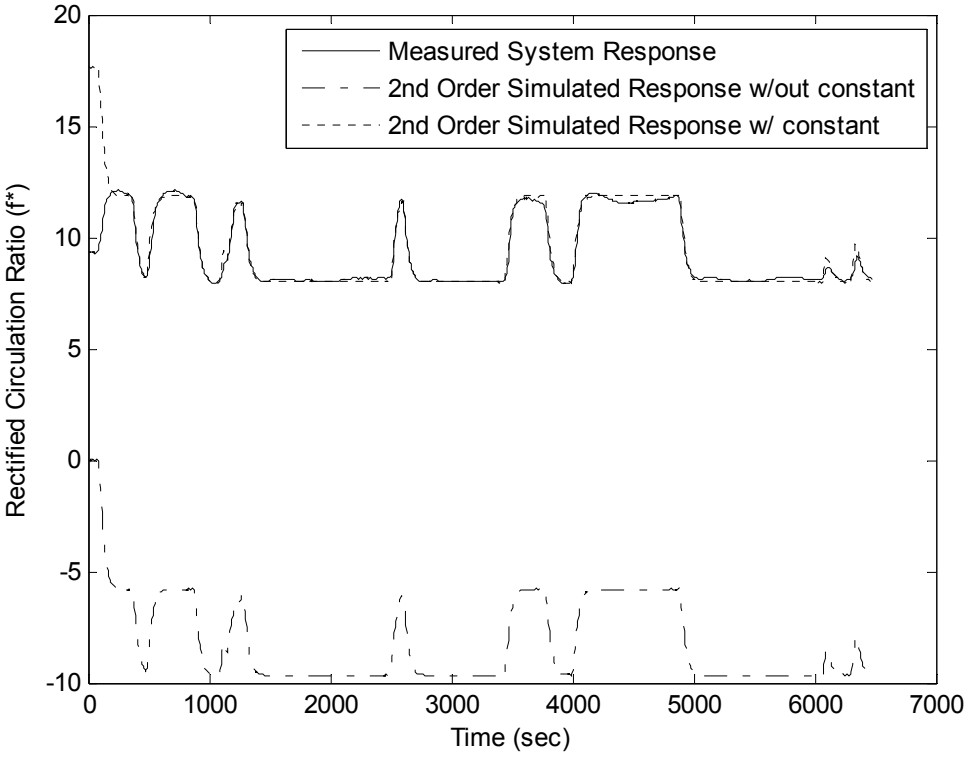

Figure 4.4: System A simulated vs. measured response for selected input

It is clear from the figure that the simulated response has the correct dynamics but has a constant bias from the measured response. The reason for the shift can be explained by examining how the simulated response is generated in MATLAB. While the system is represented as the transfer function $P2D = \frac{ke^{-\theta s}}{(1+\tau_1 s)(1+\tau_2 s)}$, the same system dynamics can be represented by an ordinary differential equation (ODE). In fact the transfer function can be rewritten into an ODE. The response is the solution to the ODE corresponding to the transfer function P2D. Recall that the solution to a particular ODE is the solution to the homogenous ODE plus a constant. The initial MATLAB simulation is the solution to the homogenous ODE. By solving for the necessary constant and including it in the calculated response, the simulated response is corrected as shown by the dotted line. Figure 4.5 below compares the 1st and 2nd order simulations for model B.

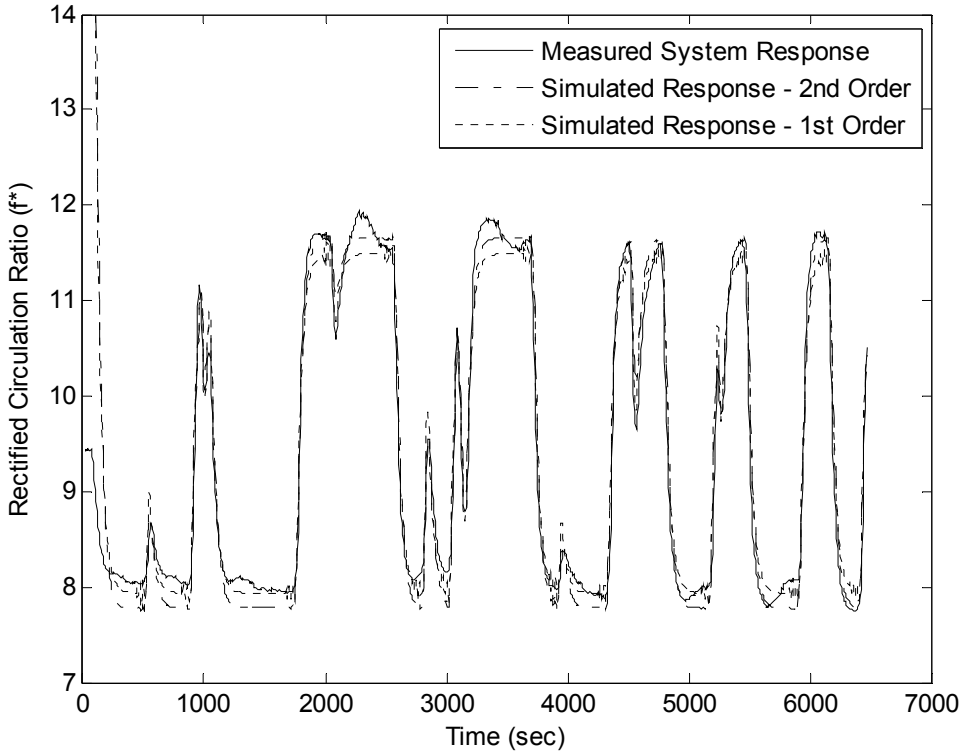

Figure 4.5: 1st and 2nd order model simulated response for selected input

From the figure it is clear that the 2nd order simulation is slightly different than the 1st order simulation with a slightly better percent fit but additional complexity. The simulation of the models in MATLAB enabled a comparison of the uncontrolled system dynamics of the desorber under the various testing conditions investigated. Figure 4.6 shows the natural step response of each model; refer to table 3.1 for the corresponding testing conditions of each model.

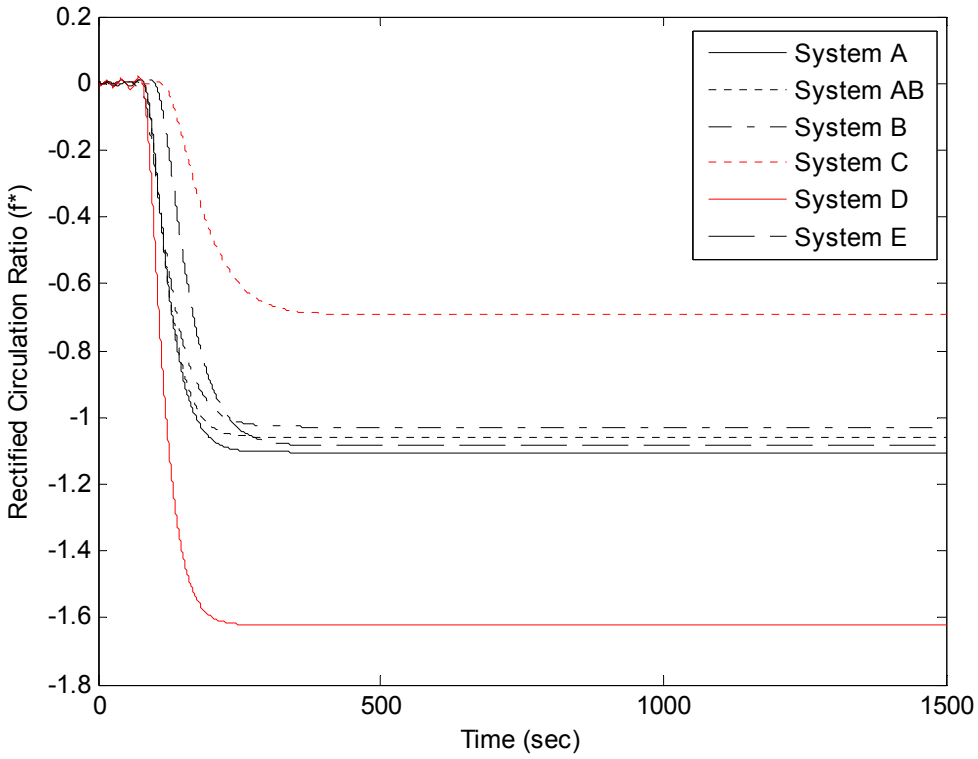

Figure 4.6: The open loop response of the models identified

The results in Fig. 4.6 illustrate that the models A, B, and AB have very similar natural dynamics. This is appropriate since all three of these models represent the natural dynamics of the desorber at operating conditions A (see table 3.1). Model E has a similar natural gain to that of models A, B, and AB with a larger delay. Model C has the largest delay and the lowest gain while model D has the smallest delay and largest gain. With the models constructed in MATLAB it was now possible to simulate and evaluate the closed loop response of the system with various controllers.

5. CONTROLLER DESIGN AND TESTING RESULTS

The linear models developed via system identification, as detailed in chapter 4, were used to design, simulate, and evaluate a variety of different controllers. Controllers demonstrating considerable improvements in operating performance via simulation were selected for experimental testing, and a single tuned controller was tested extensively.

5.1. Controller Design

While SISO systems offer an opportunity to implement a variety of control methodologies (PID, gain scheduling, model predictive control, fuzzy logic controllers), PID control is investigated in this study due to its simplicity in implementation, required hardware, necessary computing power, and design. Additionally, research regarding the design, performance, and stability of PID controlled systems is relatively mature as compared to alternative control methodologies. Despite their simplicity, PID controllers are commonly implemented as a control solution for industrial applications.

5.1.1. Ideal PID Controller Constants

Research into the design of PID controllers has identified processes for selecting controller gains that result in a closed loop system response with an appropriate balance between fast rise time (T_r), settling time (T_s) and low percent overshoot ($\%OS$) and robustness to noise. While the tuning rules of Ziegler and Nichols [23] are often used, Skogestad [17] developed an alternative set of rules for calculating the ideal gain constants for a PID controller. In this methodology, the system

dynamics are approximated by a first- or second-order time delay model. The fact that the desorber dynamics are well represented by such a model, lead to the consideration of these tuning rules for controller design. The Skogestad tuning rules are based on the model of the plant dynamics. The ideal PID controller constants for the 2nd order models (P2D) of the system are:

$$K_c^{'} = \frac{0.5}{k}\frac{(\tau_1 + \tau_2)}{\theta}; \quad \tau_I^{'} = \tau_1 + \tau_2; \quad \tau_D^{'} = \frac{\tau_2}{1 + \frac{\tau_2}{8\theta}}, \tag{36}$$

where k, τ_1, and τ_2 are from equation (32) and, $K_c^{'}$, $\tau_I^{'}$, and $\tau_D^{'}$ are the gains of the PID controller. The gains can be alternatively expressed as k_p, k_i, and k_d by using equation (4). For the 1st order system (P1D) the gains are calculated in the same manner, however $\tau_2 = 0$ for the system and the equations simplify to:

$$K_c^{'} = \frac{0.5}{k}\frac{(\tau_1)}{\theta}; \ \tau_I^{'} = \tau_1; \ \tau_D^{'} = 0. \tag{37}$$

Thus, according to the Skogestad tuning rules, the ideal PID controller for a 1st order system is in fact a PI controller. It is important to note that these tuning rules only provide a starting point in controller design. After validating system performance with specific controller gains via simulation, experimental testing was used to refine the controller gains. Experimental tuning of controller gains is important in obtaining acceptable system performance, since the model only captures a percentage (up to 89% in this case) of the underlying system dynamics.

5.1.2. Implementation in LabVIEW

The PID controller was implemented in the experimental setup using LabVIEW, since LabVIEW is already utilized to perform data acquisition and calculate the output variable of interest, f*. Since digital control is utilized in this investigation, a discrete formulation of the PID controller is required for implementation. A discrete parallel form of the PID controller for the desorber was developed from relationships provided in [16], which results in a controller in terms of the variables of this study, of the form

$$u(t) = u(t-1) + k_p[f^*(t) - f^*(t-1)] + k_i T_s e(t) + \frac{k_d}{T_s}[f^*(t) + f^*(t-2) - 2f^*(t-1)]. \quad (38)$$

In equation (5.3) $u(t)$ is the pump voltage at time t and T_s is the sampling period of the control. This equation was integrated into LabVIEW code for use in the controller validation testing.

5.1.3. Simulation

Equation (5.1) was used with the models obtained from the identification process to calculate controller gains for each model, as summarized in Table 5.1.

Controllers designated by the letters, A,C,D, or E were developed by applying the skogestad tuning rules to the corresponding model of the desorber under the corresponding operating conditions.

Table 5.1 Skogestad Gains for the models

Model Used for Calculation	Controller Name	k_p	k_i	k_d	τ_D	τ_I
A	A	-0.257	-0.006	-2.985	46.429	11.605
B	B	-0.372	-0.007	-5.255	56.483	14.121
C	C	-0.496	-0.006	-9.668	78.043	19.511
D	D	-0.157	-0.004	-1.579	40.173	10.043
E	E	-0.285	-0.005	-4.439	62.293	15.573

With the gains calculated, PID controllers were coupled with their respective models and the closed loop response was simulated in MATLAB. The following notation was used for identifying a simulation or test with the operating conditions and controller used:

$$\text{Operating Condition}\ {}^{\text{Model/Exp.}}_{\text{Controller}}.$$

With superscript xm and exp designating the order of the model or experimental results. Subscript NC representing "no control" or an open loop response. Examples of the notation are: A_A^{2m}, A_c^{EXP}, A_{NC}^{1m}. The simulated open loop and closed loop unit step response of operating conditions A, systems A_{NC}^{2m} and A_A^{2m} respectively, are shown in Fig. 5.1. The simulated open loop and closed loop response of operating conditions D, systems D_{NC}^{2m}, D_D^{1m}, and D_D^{2m} are shown in Fig. 5.2 . While the open loop responses of the modeled systems were previously illustrated in figure 4.5, they are reproduced here to illustrate the significant difference in system response obtained with the addition of a PID controller.

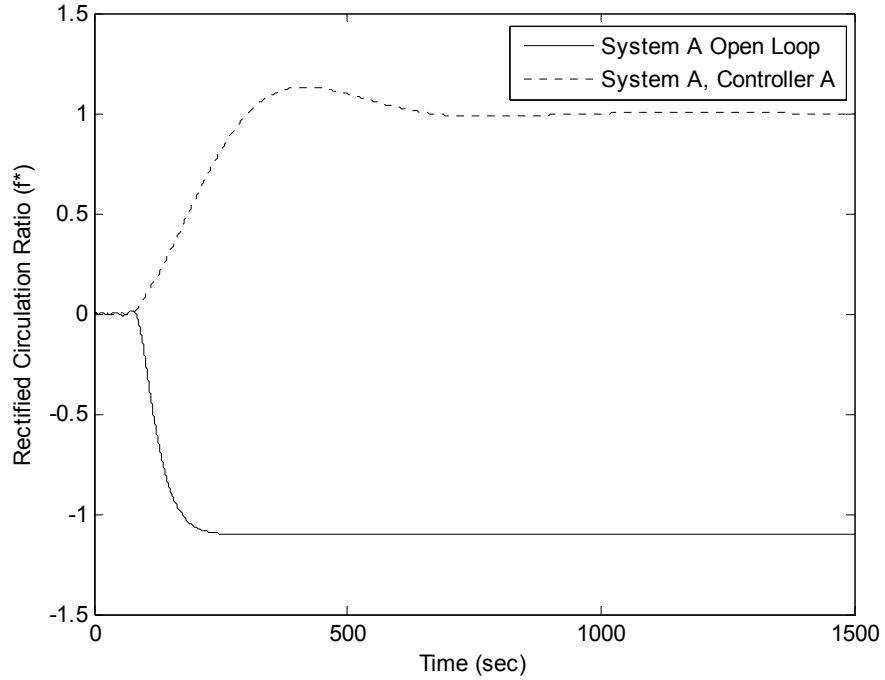

Figure 5.1: Simulated unit step response of systems A_{NC}^{2m} and A_{A}^{2m}

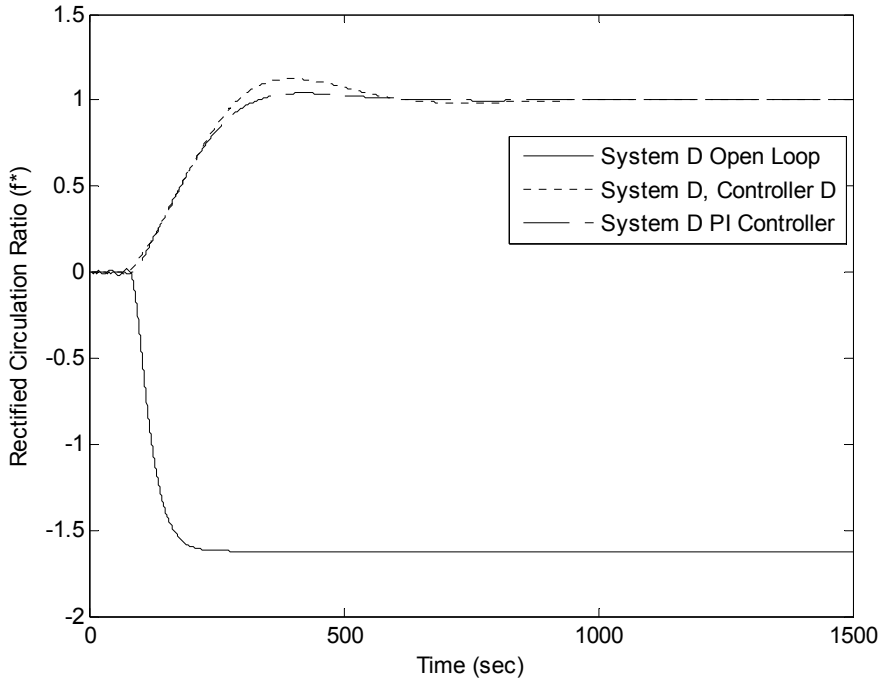

Figure 5.2: Simulated unit step response of systems D_{NC}^{2m}, D_{D}^{1m}, and D_{D}^{2m}

The responses illustrated in Figures 5.1 and 5.2 are representative of all the models investigated. These figures illustrate that the main benefit of control, in this instance, is the zero steady state error that is achieved. Control will therefore enable operation near desired f* values, resulting in an improvement to the absorption refrigeration cycle COP. This improved performance comes at a cost, though, since there is an increase in the rise time of the closed loop systems and the introduction of over-shoot. Table 5.2 summarizes the open and closed loop responses for each model and its controller.

Table 5.2 Open and closed loop response comparison

	System Response			
System Notation	Rise Time (sec)	%OS	Settling Time (sec)	Stead State Value
A_{NC}^{2m}	78.2	0	217	-1.1
A_{A}^{2m}	168	13.1	616	1
B_{NC}^{2m}	94.8	0	328	-1.03
B_{B}^{2m}	163	15.2	804	1
C_{NC}^{2m}	131	0	341	-0.0693
C_{C}^{2m}	244	14.5	1180	1
D_{NC}^{2m}	67.8	0	196	-1.62
D_{D}^{2m}	159	12.5	583	1
E_{NC}^{2m}	105	0	282	-1.09
E_{E}^{2m}	211	13.8	773	1

From table 5.2 it can be seen that when control is added to the system under any of the operating conditions the rise time increases, overshoot is added to the response and the settling time greatly increases. The trade-off, which makes control desirable,

is that the controlled systems reach the desired value (1 for a unit step) instead of having the significant steady state errors which exist for each open loop system.

While the Skogestad tuning rules can be used to determine the ideal gains for a given plant, the actual desorber will be operated in a variety of conditions and within some range about the designed operating state. Gain scheduling could be utilized to vary controller gains in a means appropriate to the operating conditions, but a single controller may also prove capable of desorber control over a range of operating conditions. As a result, the next step in the controller design was to simulate the closed-loop response of the various models when implemented with a single controller. The relative quickness of the simulations enabled calculation of all possible combinations of models and controllers resulting in 25 different additional model / controller combinations, e.g. A_C^{2m}.

These simulations of the closed loop response are utilized to identify appropriate gain values that can serve as a starting point for the physical implementation of the controller on the desorber. Appropriate gain values were identified primarily through their influence on the rise time and percent overshoot of the closed loop system, resulting in a band control strategy. Settling time, T_s was not weighted as heavily in this analysis since the inclusion of an integral term in the controller will eventually result in zero steady state error. Additionally, since the open loop system would typically operate away from the desired f* state, controlled system operation near the desired rectified circulation ratio represents a vast improvement over the alternative. As a result, quickly obtaining the exact desired

value was not necessary to obtain performance improvements. Table 5.3 shows the responses for the various model and controller combinations that showed promise for the physical controller. The complete table containing all combinations is included in Appendix 9.

Table 5.3: Simulated closed loop response of the most promising controller/model systems

	Closed Loop System Response				
	Rise Time (sec)	%OS	Settling Time (sec)	Stead State Value	Delay Estimate (sec)
A_A^{2m}	168	13.1	616	1	77
A_C^{2m}	162	9.93	567	1	76.5
A_D^{2m}	256	2.65	689	1	77
B_B^{2m}	163	15.2	804	1	70
B_C^{2m}	184	8.63	615	1	69.5
B_D^{2m}	288	1.76	495	1	70
C_C^{2m}	244	14.5	1180	1	107
C_D^{2m}	403	2.55	1080	1	108
D_C^{2m}	94	17.6	636	1	73.5
D_D^{2m}	159	12.5	583	1	74
E_C^{2m}	154	24.6	950	1	95
E_D^{2m}	234	11.2	855	1	95.5
E_E^{2m}	211	13.8	773	1	95

Inspection of the table reveals that controller C has very low rise times for all five models, while controller D has the lowest $\%OS$ for each simulated model. The Skogestad recommended controllers, systems A_A^{2m}, B_B^{2m}, etc. are also included as a gauge for "good" closed loop response of that model.

5.1.4. Controller Selection and Refinement

Informed by the controller simulation results, physical testing of controllers C and D was performed on the actual system under operating conditions characteristic of A, (A_C^{EXP} and A_D^{EXP}). Figures 5.3 and 5.4 illustrate the closed-loop response of both the simulation and experimentation (A_C^{2m} and A_C^{EXP}) and (A_D^{2m} and A_D^{EXP}) for a chosen desired desorber variation in f*.

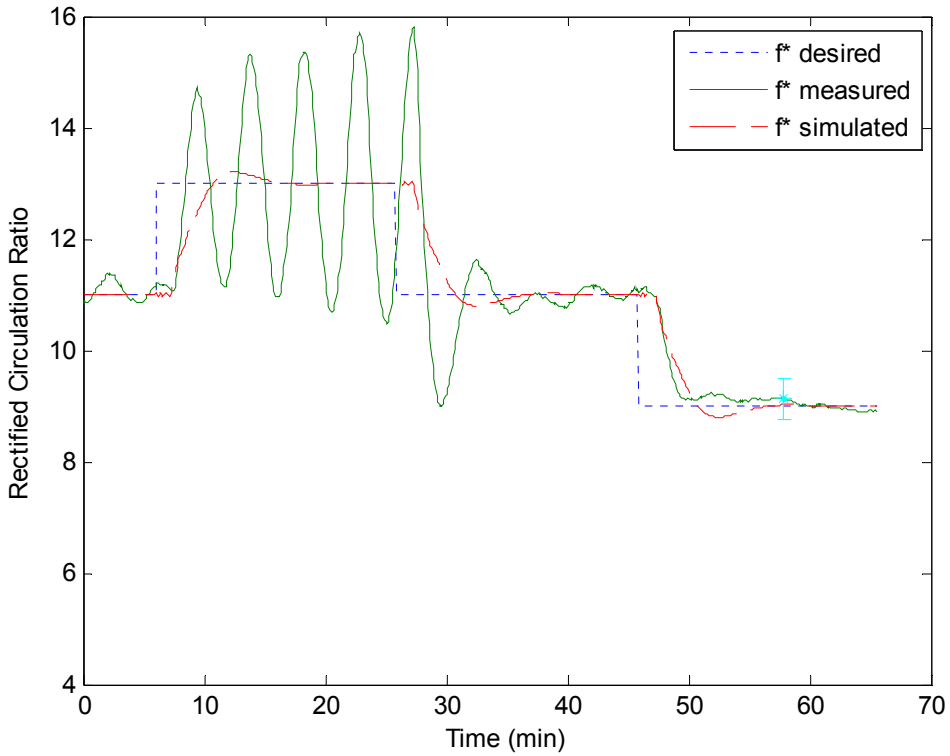

Figure 5.3: Simulated and measured responses for systems A_C^{2m} and A_C^{EXP} respectively

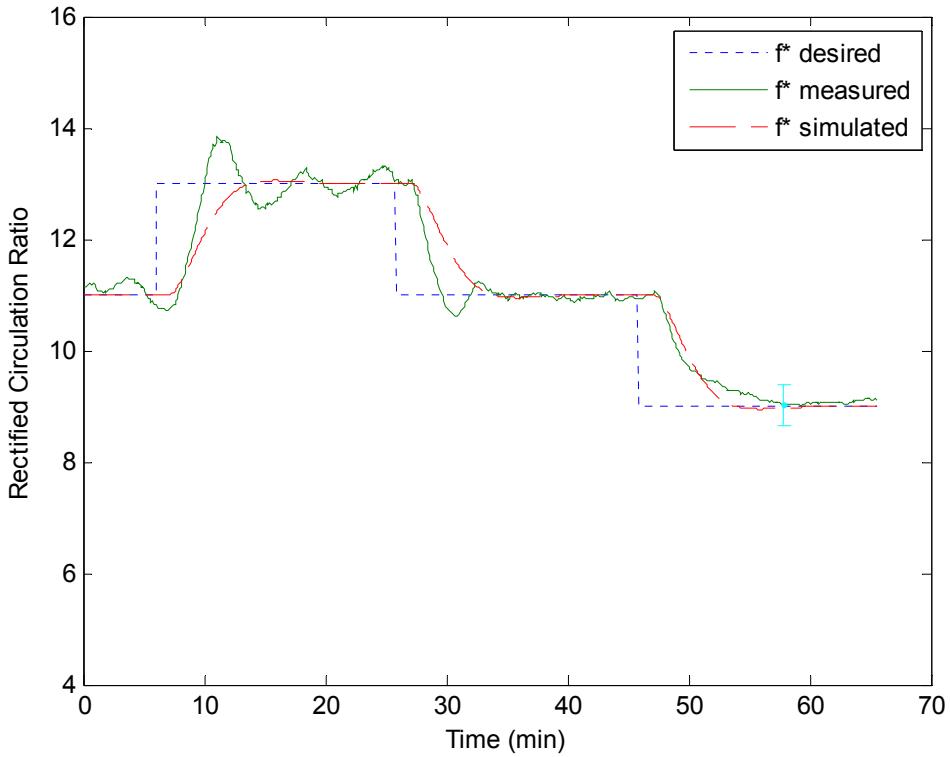

Figure 5.4: Simulated and measured responses for systems A_D^{2m} and A_D^{EXP} respectively

It is clear from the large increasing oscillations in figure 5.3 that the measured and simulated results vary widely in their agreement. For f* = 13 the qualitative nature of the responses are very different and the increasing oscillations of the measured response appears to indicate instability. Yet, for f* = 9 the simulated and measured results match very well. In figure 5.4 the simulated and measured results agree both qualitatively and quantitatively, although the measured response appears to have more overshoot and a faster rise time.

Based on these initial results the controller gains were further tuned on the actual system to try to achieve a controller that inherited the rise time of the C controller and the lower overshoot of the D controller. This tuning procedure yielded

final gains of: $k_p = 0.3$, $k_i = 0.003$, and $k_d = 2.0$, and the controller with these gains is referred to as the "tuned" controller and is designated with a T subscript. Figure 5.5 illustrates the closed loop response of model A with the various controllers investigated during the tuning process.

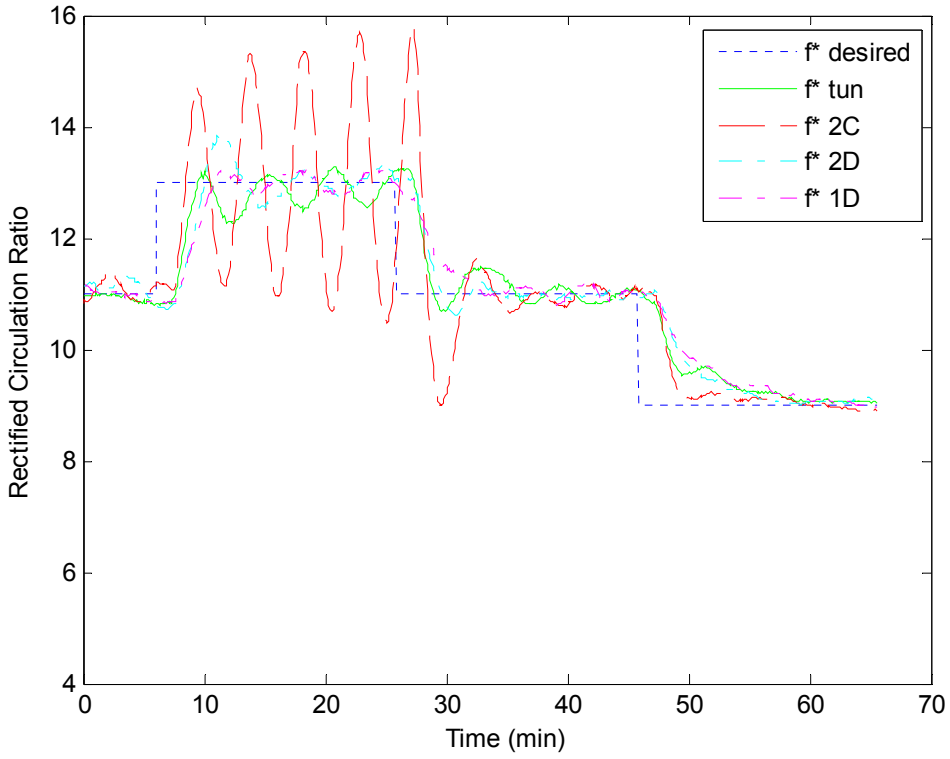

Figure 5.5: Measured Responses for systems A_T^{EXP}, A_C^{EXP}, A_D^{EXP}, $A_{D\_PI}^{EXP}$

Qualitative analysis of the results indicate that the system A_C^{EXP} has very high overshoot, system $A_{D\_PI}^{EXP}$, (a PI controller), has the slowest rise time, and system A_D^{EXP} has a slower rise time and more overshoot than A_T^{EXP}, the tuned controller. The tuned controller represents a good compromise between low $\%OS$ and a faster T_r

and was chosen as the controller for additional testing. These results further illustrate the need to use simulation as a starting point for testing on the physical system.

5.2. Controller Validation Tests

Tests were designed to answer the following two questions about the chosen controller, controller T:

1. can the controller control the system through the range of operating conditions investigated?
2. how robust is this controller to disturbances?

This additional testing was necessary because the relationship between the oil mass flow rate and the rectified circulation ratio is complex and nonlinear, yet it is being approximated by a simple linear model which only explains ~85% of the variation seen in the data. Additionally, noise encountered in system operation may affect controller performance. To investigate the controller performance, a series of step responses were chosen. A well-controlled system would track the desired value of the rectified circulation ratio, f*. Controller performance for variation in operating conditions was investigated by testing the controller on the four different operating states used in this investigation (see table 3.1).

A measure of the robustness of the controller is determined by examining its ability to regulate about a desired value in the presence of an introduced disturbance. In a real application the desorber would be designed for a given strong solution flow rate, oil temperature, operating pressure, etc. However, during normal operation these and other design parameters may not always remain at the values for which the

cycle was designed, e.g. the strong solution flow rate may fluctuate. As a result, for improvements in the system performance, the controller must be able to effectively reject these types of disturbances and maintain f* at the desired value. An example of a disturbance investigated in this work is a variation of the mass flow rate from 35 to 25 g/min. In this and other disturbances to strong solution flow rate, oil temperature, and manifold pressure, we wish to determine how well the controller maintains the desired rectified circulation ratio, f*.

5.2.1. Operating Procedures for Controller Testing

These procedures are different than those used for the system identification testing, although both the startup and shutdown of the experimental testing device remain the same. The detailed procedures are included in Appendix 4. Once the system has been brought to steady state, the oil flow rate controller was activated and the controller test began. All controller tests, regardless of their differences, try to maintain the rectified circulation ratio at specific values. Therefore, very little operator involvement was necessary during the tests. Strong solution flow rate, oil temperature, manifold pressure, and hold up volume were all monitored during each test and adjustments to each were made as necessary.

5.3. TRACKING TEST RESULTS AND DISCUSSION

Tracking tests were conducted to validate controller performance on the actual desorber system. Tracking tests were performed at each of the testing states from table 3.1. Because of the differences in strong solution flow rate and oil temperature between testing states, the desorber system could not reach the same

rectified circulation ratios in all four cases. As a result, three different tracking tests were used. Figure 5.6 shows the tracking test results for systems A_T^{EXP} and D_T^{EXP}. The nominal values for each operating condition are found in table 3.1 or figure 5.11 which follows later in the chapter. As can be seen from figure 56, both systems begin with a rectified circulation ratio of approximately 11. The desired response is a series of steps in the rectified circulation ratio from 13 to 11, and then from 11 to 9. Controller T is used for control in both experiments.

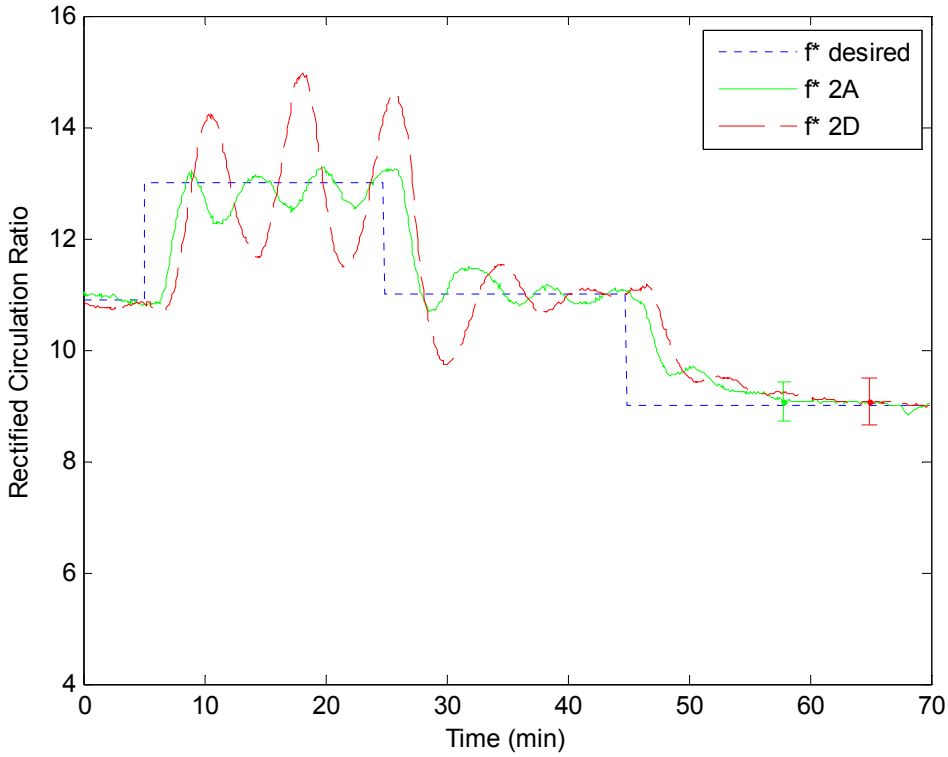

Figure 5.6: Measured tracking results for systems A_T^{EXP} and D_T^{EXP}

Fig 5.6 clearly illustrates that the desorber system is controlled and follows the desired path. However, the behavior of systems A_T^{EXP} and D_T^{EXP} are quite different.

Controller T was tuned for operating conditions A previously so it is not surprising that it performs better when applied to conditions A than conditions D. It is surprising that controller T controls the desorber under conditions D when they vary from the tuned conditions by 33% in Mss and 9% in Toil. It is also interesting that the system responses are different depending on the ending rectified circulation ratio. The response for both models is best when changing to f* = 11. This change in the response behavior can be explained by the nonlinear nature of the system being controlled. The controller gains were chosen based on a linear approximation of the system determined from the system identification process. Recall that in the identification process the oil flow pump rate was varied from 5.25 to 8.75 volts. The response in changing to f* = 11 results in good performance for both systems A_T^{EXP} and D_T^{EXP} since the corresponding oil flow rate voltage to f* = 11 lies between 5.25 and 8.75 Volts for both operating conditions. In contrast, the rectified circulation ratios of 13 and 9 lie near the edge or outside of the boundaries of the area where the linear approximation of the system is valid. Both closed loop systems appear to be under-damped or unstable at f =13 and over-damped at f* = 9. Additionally, it was observed during the testing that a high rectified circulation ratio of 13 corresponded to very little vapor production. In this scenario, the system nonlinearities appeared to have increased relevance than for lower f* values, since very small changes in the oil flow rate began to show much larger changes in f*. This behavior of the desorber under both operating conditions explains the larger oscillations that are observed at this value.

Figures 5.7 and 5.8 illustrate the results of the same tests for systems C_T^{EXP} and E_T^{EXP}. In both of these tests the desired f* values were adjusted to represent the range of rectified circulation values that the desorber was capable of achieving for the operating condition. The results of the tests for both systems C_T^{EXP} and E_T^{EXP} are similar to those observed for systems A_T^{EXP} and D_T^{EXP}. The same change in the response nature from higher to lower rectified circulation ratio values is observable, and both systems have the best response at their corresponding "middle" test value.

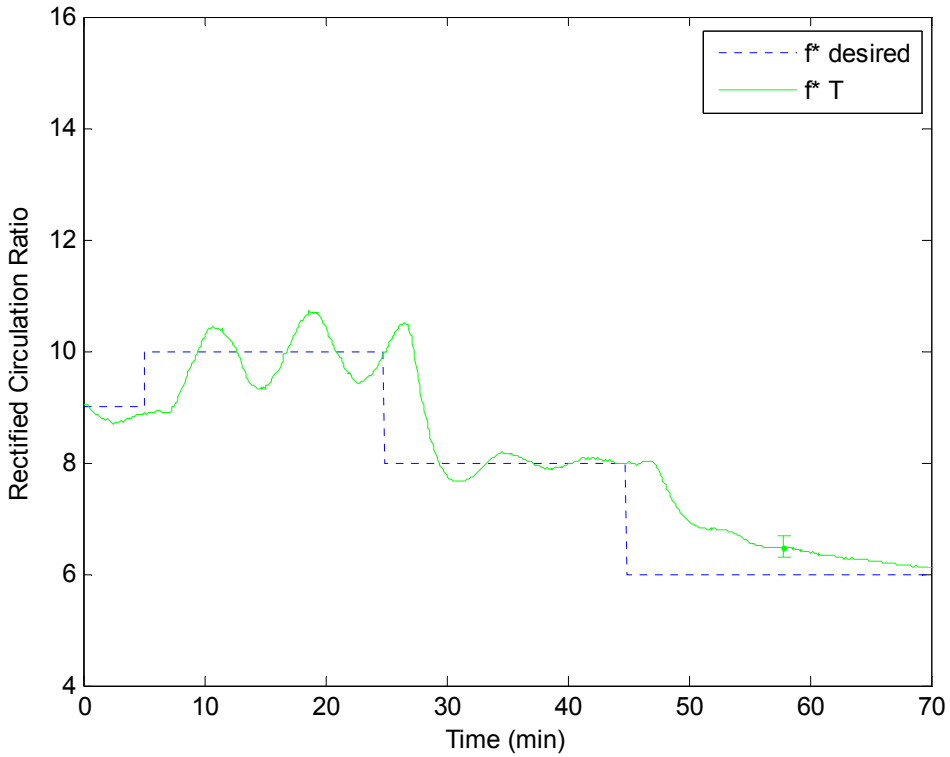

Figure 5.7: Measured tracking results for system C_T^{EXP}

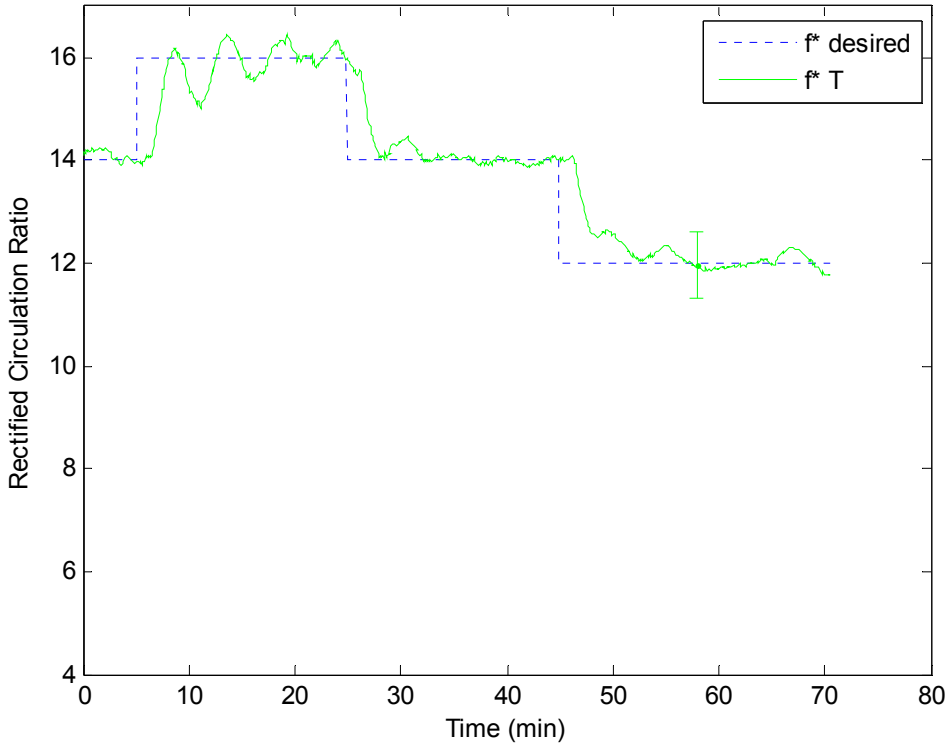

Figure 5.8: Measured tracking results for system E_T^{EXP}

It is interesting to note that both system A_T^{EXP} and E_T^{EXP} have significantly lower oscillations at their respective "higher" f* test values than systems C_T^{EXP} and D_T^{EXP}. Both systems A_T^{EXP} and E_T^{EXP} had strong solution flow rates of 35 g/min, so it is reasonable to conclude that changing the strong solution flow rate has a greater affect on the desorber dynamics at higher rectified circulation ratios than does changing the oil temperature. This is especially useful knowledge from a design perspective because in a real system the strong solution flow rate is much more likely to vary faster and more frequently than the oil temperature.

System A_T^{EXP} was tested in the reverse direction and the results are illustrated in Fig 5.9. Comparing the response of system A_T^{EXP} in figures 5.6 and 5.9 the following observations can be made.

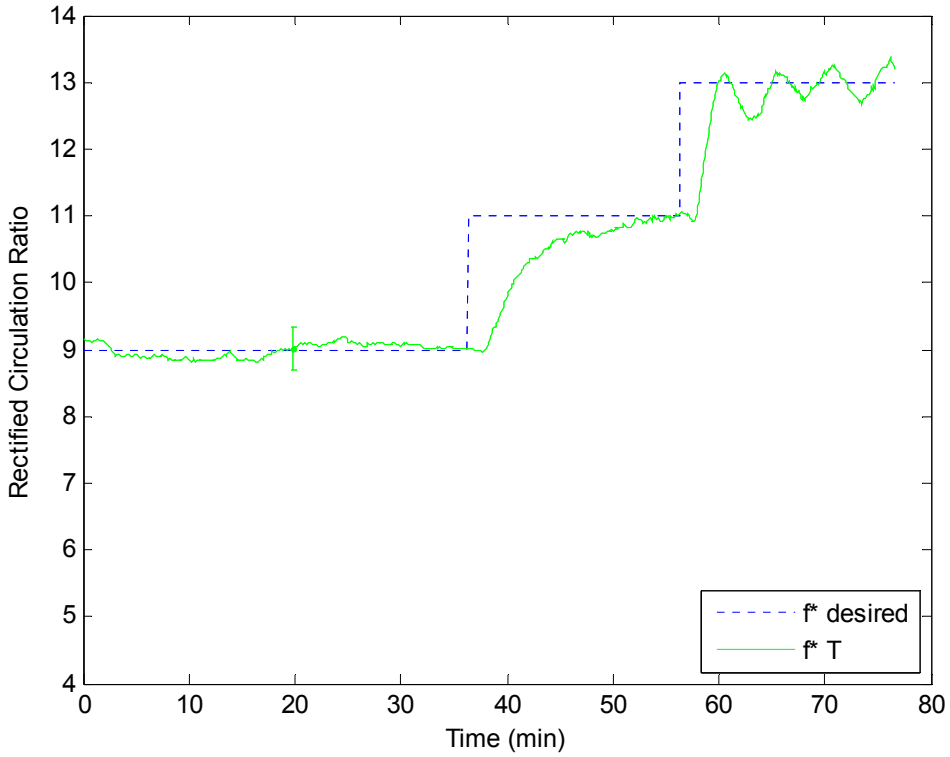

Figure 5.9: System A_T^{EXP} tracking a stair signal in the reverse direction

The response in the desorber stepping to f* = 11 from a higher f* values has a faster rise time and more overshoot than the response stepping from a lower f* value. This is explained by modeling error resulting from a linear approximation of a nonlinear relationship. While the response varies the system is controlled regards of the stepping direction. Below Figure 5.11 shows the response of system A_T^{EXP} to a

modified tracking signal. The desired f* value gradually varies between high and low values rather than the discontinuous steps of the earlier tests.

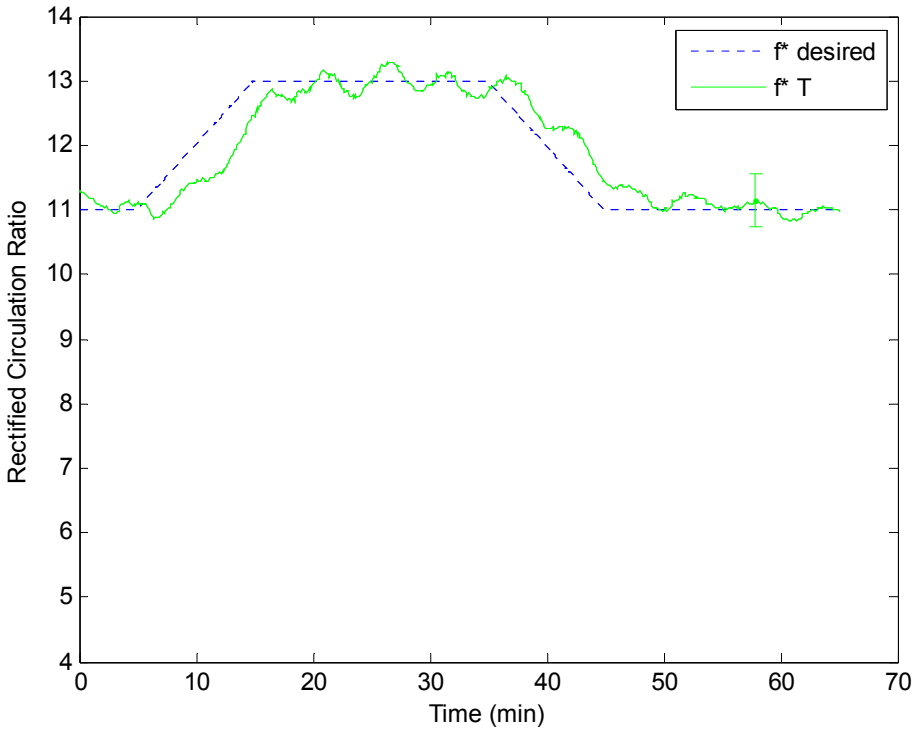

Figure 5.10: System A_T^{EXP} tracking a ramping signal

While the oscillations and overshoot observed in the step responses remain, this test illustrates that the controller is capable of tracking variations in f* that might be specified for a specific application. The delay in the system is apparent in the shift to the right in the measured response and can not be eliminated regardless of the control gains used.

The ability of the tuned controller to track the desired signals for each of the four operating conditions investigated shows that a simple PID controller is able to

control the desorber over a fairly wide range of operating conditions. While the closed-loop system performance varied depending on the operating conditions, the single PID controller was able to effectively regulate the desorber operation about the desired f* values. As well, it was also robust against the modeling error and noise present in the systems tested.

5.4. ROBUSTNESS TEST RESULTS AND DISCUSSION

In a physical implementation, the controller must maintain performance despite disturbances in model parameters. While the purpose of this research was not to design a "robust" controller, the robustness of the designed controller was investigated with the following tests. Figure 5.11 illustrates the various disturbances that were introduced into the desorber during testing to measure the robustness of the controller. A robust controller will maintain the desired f* in spite of disturbances.

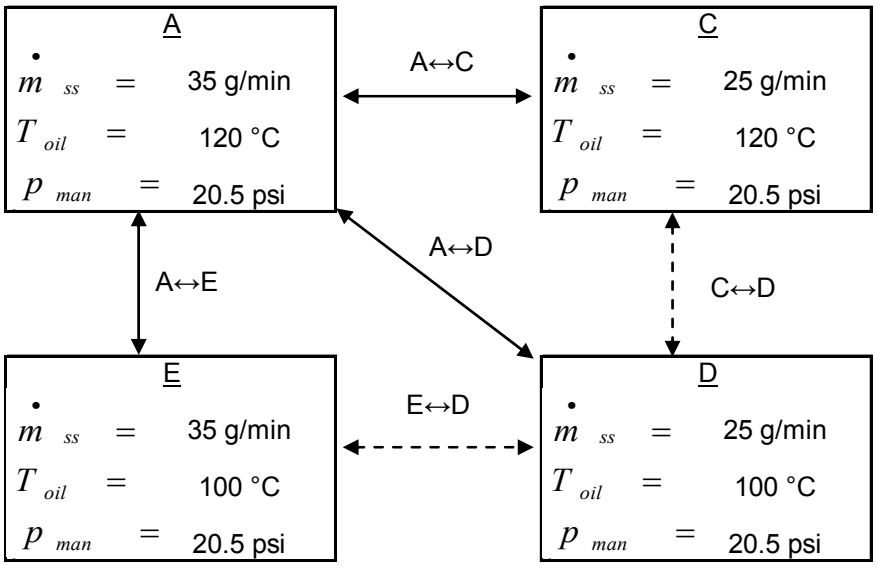

Figure 5.11: Robustness tests between operating conditions

Fig. 5.11 shows the 10 robustness tests that were conducted by introducing disturbances into the system. The disturbances introduced were changes in strong solution flow rate or oil temperature that changed the system from one set of operating conditions to another. For example test D→E changed $\dot{m}_{ss}$ from 35 to 25 g/min. While all the tests shown in Fig. 5.11 were conducted, the dashed line test results are not illustrated in the chapter as they followed the trends of the other tests.

5.4.1. Strong Solution Flow Rate Disturbances

The ability of the controller to maintain a constant f* during a 10 g/min step change in the strong solution flow rate was investigated . Figures 5.12 and 5.13 show the results of tests A→C and C→A respectively. See figure 5.11 for the nominal operating conditions of the tests.

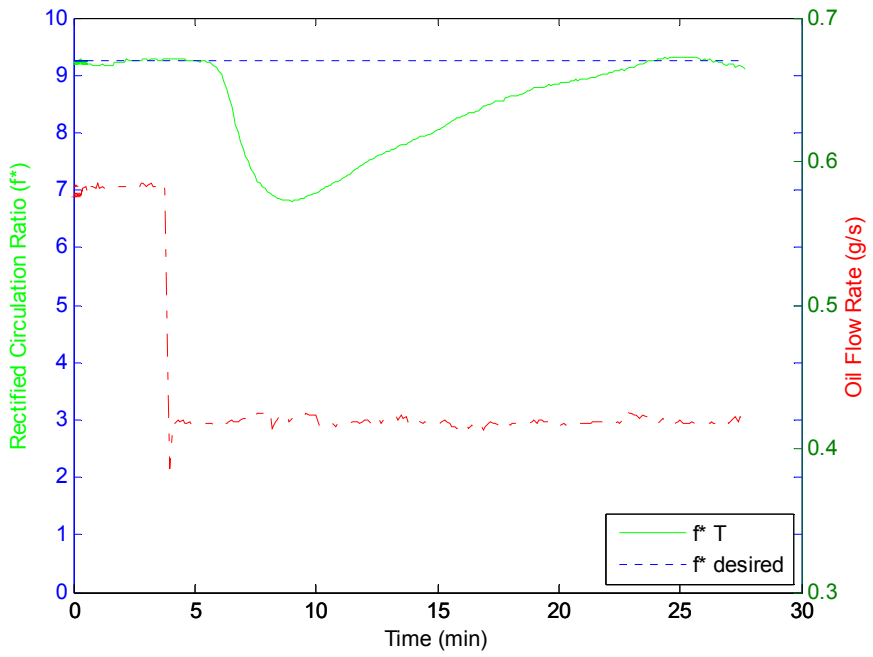

Figure 5.12: Robustness test changing operating conditions from A→C

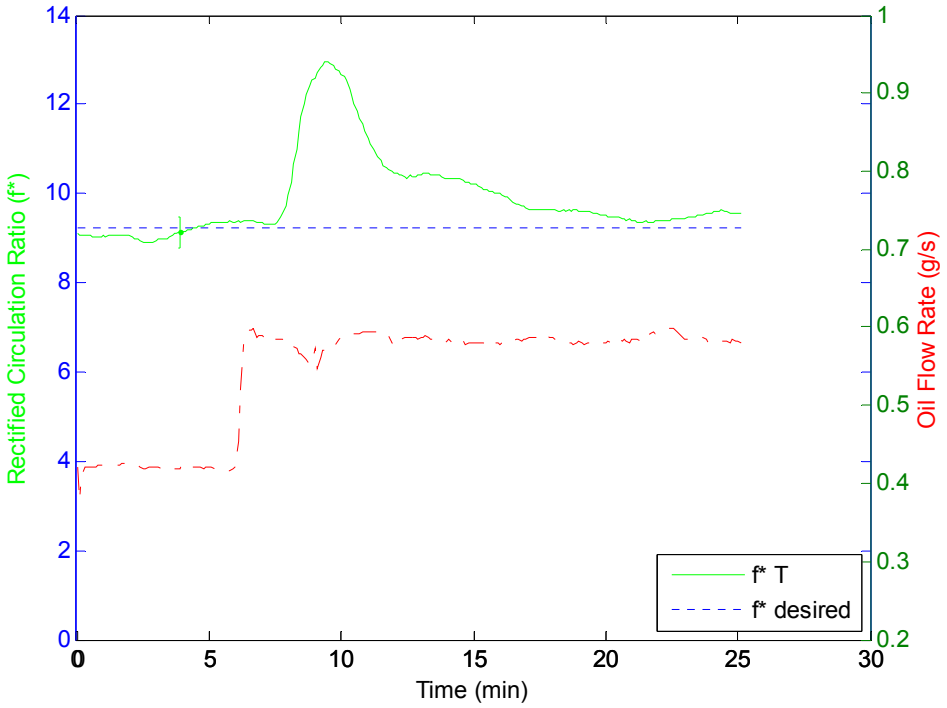

Figure 5.13: Robustness test changing operating conditions from C→A

In both tests the variation in $\dot{m}_{ss}$ had a large and rapid effect on f* as hypothesized previously. The settling time for both disturbance tests is similar to that obtained in the step tests at a single operating condition. The behavior of the closed loop system in changing from A→C and C→A is qualitatively similar with both systems changing f* by approximately 3 before the controller begins to regulate the system back to the desired value of 9.25. The disturbance tests from operating conditions E→D and D→E yielded the same qualitative results, although the change in f* varied more in changing from D→E than from E→D. As in the A↔C tests the PID controller was able to regulate the system output back to the desired f* value.

5.4.2. Oil Temperature Disturbances

Oil temperature disturbances to the system were also investigated. Since it is impossible to introduce a step change in the oil temperature both figures 5.14 and 5.15 were conducted for an approximately linear variation in the oil temperature with other parameters help constant. The figures correspond to changing from operating conditions A→E and E→A respectively.

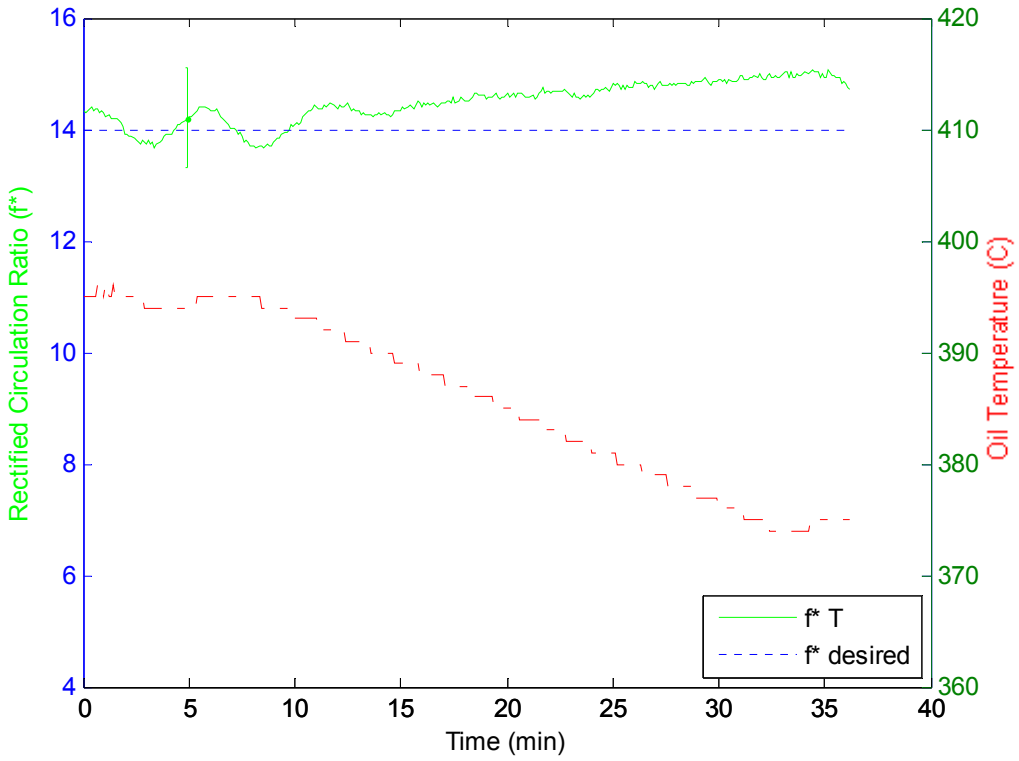

Figure 5.14: Robustness test changing operating conditions from A→E

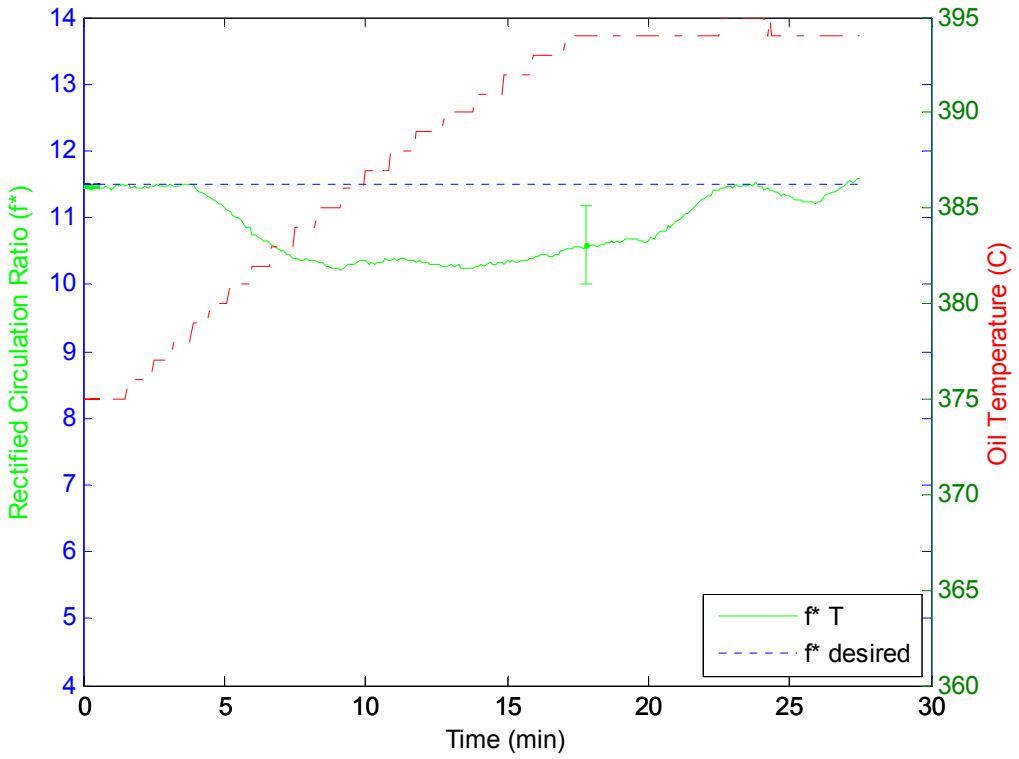

Figure 5.15: Robustness test changing operating conditions from E→A

Examination of the results reveals that the change in f* is not as drastic as that observed with the $\dot{m}_{ss}$ change. This may partially be due to the gradual nature of this change as opposed to the step change in the $\dot{m}_{ss}$ disturbance. The low maximum errors between the desired and controlled output show that the controller is able to regulate f* n the presence of disturbances to the oil temperature. It is likely that this result is due to the choice of controlled input $\dot{m}_{oil}$. The rectified circulation ratio, f*, is dependent on the applied heat flux to the desorber, which is a function of both T_{oil} and $\dot{m}_{oil}$. The applied heat flux can be maintained despite of disturbances in Toil by

adjusting $\dot{m}_{oil}$. This is different than the effect of $\dot{m}_{ss}$ disturbances, where changing $\dot{m}_{oil}$ will compensate for the disturbance, but does nothing to reduce or eliminate the disturbance.

5.4.2.1. Additional Disturbances

For the controller to function appropriately in an actual system, it will need to be robust to all possible disturbances and noise simultaneously. A more realistic testing scenario therefore involves simultaneous variations in $\dot{m}_{ss}$ and T_{oil}. Figures 5.16 and 5.17 illustrate the controlled system response in these instances as the system is varied between operating conditions A→D and D→A respectively.

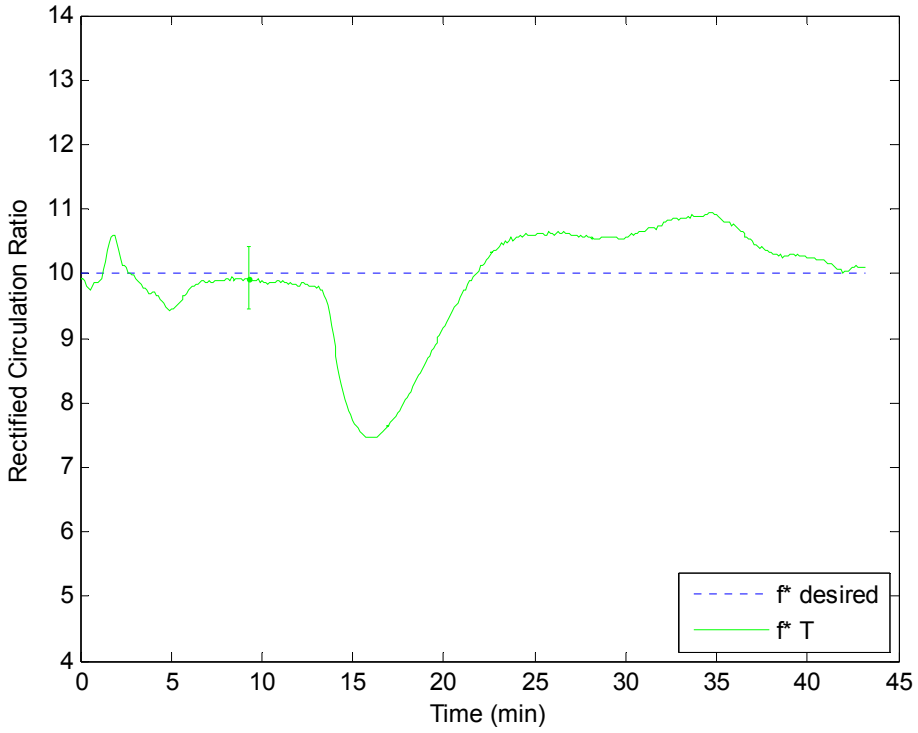

Figure 5.16: Robustness test changing operating conditions from A→D

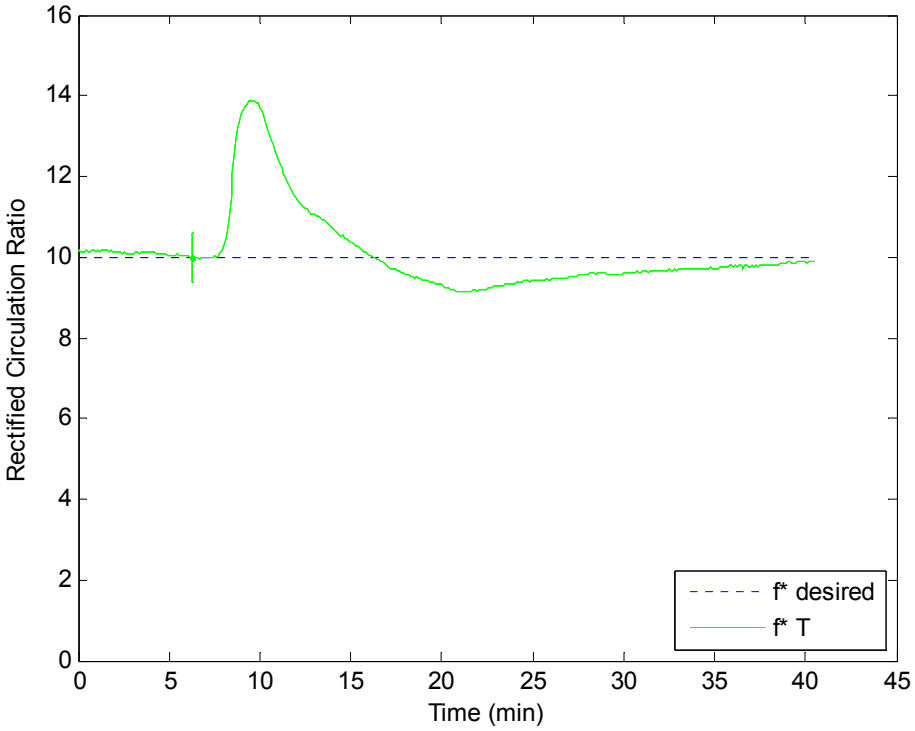

Figure 5.17: Robustness test changing operating conditions from D→A

The f* response in fig 5.17 looks very much like the superposition of figures 5.13 and 5.15. This is surprising because the system is not linear. Figure 5.16 also appears to be the superposition of the two separate disturbances which were shown in fig. 5.12 and 5.14. In both tests the controller was able to compensate for the disturbances present and regulate the desorber rectified circulation ratio back to the desired value. Recall that f* does not need to be at the precise desired value for the benefits of the controller to be present. For example, in 5.17 f* is very close to the desired rectified circulation value after approximately 8 min of introducing the disturbance.

To determine the effect of pressure disturbances, the manifold pressure was varied between 22 and 18 psi while $\dot{m}_{ss}$ and $\dot{m}_{oil}$ were kept constant at 35 g/min and 120 °C respectively. These conditions are those of operating conditions A with the introduction of the manifold pressure disturbance. Before the disturbance test was performed the pressure was varied without control. Varying the manifold pressure from 20.5 to 22 psi may have increased f* by 0.5 although it is close to the range of uncertainty in this test. Reducing the pressure to 18 psi reduced f* by 1.1. Thus, for the small pressure disturbance range tested, f* increases with increasing pressure and decreases with decreasing pressure. Figure 5.18 illustrates the results of introducing the same pressure disturbances into the system with control.

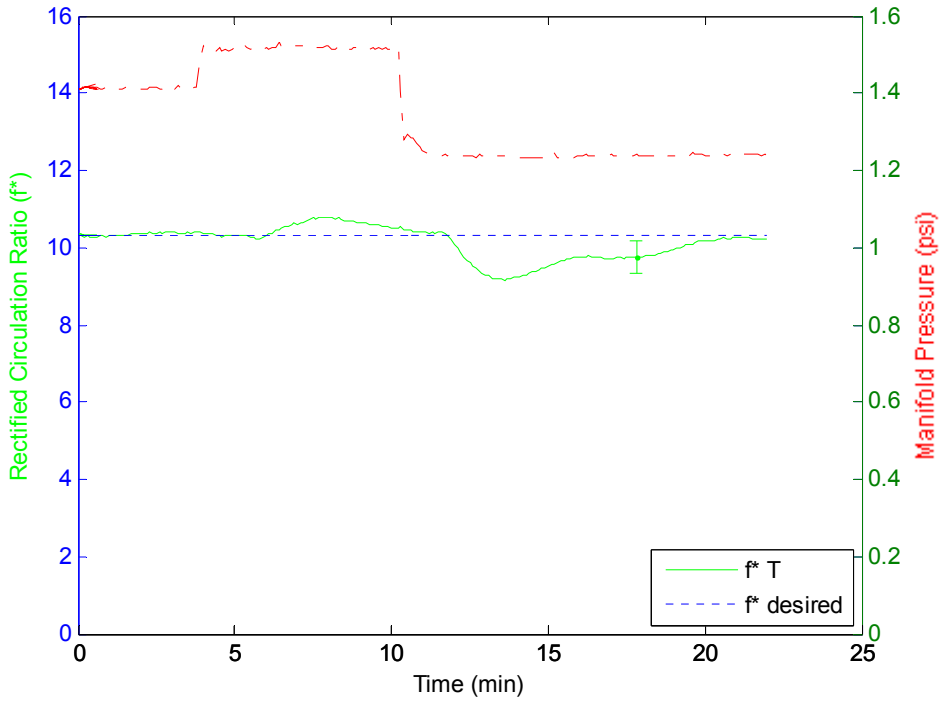

Figure 5.18: Robustness test varying P_{man}

As was the case with both the $\dot{m}_{ss}$ and T_{oil} disturbances, the controller is able to regulate to the desired value in the presence of manifold pressure disturbances as well. The controller was able to regulate f* back to the desired value with a settling time faster than observed from the other tests. The reduced settling time of the closed loop response for this test can be attributed to the small variations in f* resulting from the range of pressure changes tested. The conclusions of the testing results follow in chapter 6.

6. CONCULSIONS AND RECOMENDATIONS

In this study, system identification tests were performed on an oil-heated fractal-like branching microchannel desorber to construct several linear models of the dynamical relationship between oil pump control voltage and rectified circulation ratio. These models were used to simulate the desorber dynamics under four different sets of operating conditions. PID controllers were designed for each model and the simulated closed-loop system performance was evaluated as a starting point for physical tuning. Controllers designed for the models developed at operating conditions C and D were identified as having the best simulated closed-loop performance and were experimentally validated on the physical system using tracking tests. In these tests, a desired rectified circulation ratio was sent to the controller, and the controlled desorber rectified circulation ratio was measured for comparison. After additional tuning, controller T was selected as a controller resulting in a good compromise between low percent overshoot and a fast rise time. Controlled system performance with controller T was subsequently examined at all four operating conditions to determine if a single controller was capable of achieving acceptable performance at all of the operating conditions of interest. Controller robustness in the presence of disturbances was tested by varying the strong solution flow rate, oil temperature, and manifold pressure away from the design conditions in various combinations.

Experimental results demonstrate that choosing the rectified circulation ratio, f*, as the controlled variable enabled the relevant desorber dynamics to be adequately

represented by a linear SISO model. While the relationship between f* and $\dot{m}_{oil}$ is actually complex and highly nonlinear, it was determined that it can be approximated with considerable accuracy by a simple 2 pole time delay system. As a result, linear control design techniques, such as the PID controller investigated in this study, are capable of producing effective control for a range of operating conditions.

The simulated closed-loop system response provided a good starting point for controller design, with the actual controller requiring only minimal additional tuning when implemented on the physical system. While the measured responses of the closed-loop system had faster rise times and more overshoot than predicted by the simulations for the operating conditions tested, the simulated closed-loop response was nevertheless representative of the measured response within the range of model linearization. However, significant deviations between the simulated and measured results occurred near the "edges" of the linearized state space. This result was not entirely unexpected, since the models developed via system identification are only representative of the underlying dynamics near the operating conditions for which they were developed. It was determined that a single PID controller was able to control the desorber and regulate the system to the desired rectified circulation ratio for all four operating conditions investigated in the study. Tuning the controller performance for a single operating condition still yielded stable closed-loop systems with good response characteristics for the other operating conditions. The resulting tuned PID controller was able to recover from disturbances of up to 33% and 9% in

$\dot{m}_{ss}$ and T_{oil}, respectively. Disturbances in $\dot{m}_{ss}$ resulted in much larger changes in the rectified circulation ratio than T_{oil} disturbances. Pressure disturbances of ±2 psi had a small effect on f* and were well controlled by the PID controller. The combined stable closed-loop regulation of f^* in the presence of external disturbances illustrates that PID control can be an effective control strategy for on an oil-heated fractal-like branching microchannel desorber.

Recommendations for future work include performing identification tests over a larger range of operating conditions which are closer to the conditions encountered in absorption cycles. This will result in a linear approximation that is valid for a larger f* range and may increase the performance of the PID controller at both higher and lower f* values by reducing overshoot and increasing rise time respectively. The trade-off will be a decrease in the closed loop response of the middle f* values. An investigation into this trade-off between closed loop response and the range of model validity may reveal if a single PID controller can be used for desorber control in an absorption refrigeration cycle. If the desired response is found to be unattainable for a single controller, a gain scheduling PID controller presents an alternative control strategy. Additional system identification would be required to determine the number of system approximations necessary to yield the desired response for the range of conditions anticipated in the refrigeration cycle.

The choice of f* as the controlled variable required the use of a computer for calculation of f* at each iteration of the controller loop. The amount of computation

required may prove cumbersome for many applications. As a result, investigating the relationship between f* and the generation (desorber) temperature (T_{Des}) may yield a well defined relationship between f* and the desorber temperature, such that the desorber temperature could replace f* as the controlled variable in the PID controller. This would provide an easily measured controlled variable, significantly reducing the computational requirements and greatly reducing the size and complexity of the desorber controller. In a desorber as small as the oil-heated fractal-like branching microchannel desorber used in this study, the choice of where and how the desorber temperature is measured would likely be critical to the identification of the relationship between f* and T_{Des}.

LITERATURE CITED

[1] Mouchka, G.A., "An Experimental Study of Co-flow Ammonia-water Desorption in an Oil-heated, Microcsale, Fractal-like Branching Heat Exhanger," Thesis, Oregon State University, Corvallis, OR, USA, 2006

[2] Çengel, Y.A., and Boles, M.A., Thermodynamics: an Engineering Approach, Fourth Ed., McGraw-Hill, New York, 2002.

[3] Garimella, S., and Christensen, R.N., "Gas-fired absorption systems for space conditioning in recreational vehicles," International Absorption heat Pump Conference, New Orleans, LA, USA, vol. 31, p. 287-294, 1993.

[4] Garrabrant, M.A., "Proof-of-concept design and experimental validation of a waste heat driven absorption transport refrigerator," *ASHRAE Transactions: Symposia*, vol. 109, p. 401-411, 2003.

[5] West, G.B., Brown, J.H., and Enquist, B.J., "A general model for the origin of allometric scaling laws in biology," *Science*, vol. 276, pp. 122-126, 1997.

[6] Pence, D.V., "Reduced pumping power and wall temperature in microchannel heat sinks with fractal-like branching channel networks," *Microscale Thermophysical Engineering*, vol. 6, p. 319-330, 2002.

[7] Didion, D., and Radermacher, R., "Part-load performance characteristics of residential absorption chillers and heat pumps," *International Journal of Refrigeration*, vol. 7, pp. 393-398, 1984.

[8] Pence, D.V., "Improved thermal efficiency and temperature uniformity using fractal-like branching channel networks," Proceedings of the International Conferences on Heat Transfer and Transport Phenomena in Microscale, Banff, Canada, pp. 142-148, 2000.

[9] Daniels, B.J., Pence, D.V., and Liburdy, J.A., "Predictions of flow boiling in fractal-like branching microchannels," Proceedings of IMECE2005: ASME International Mechanical Engineering Congress and Exposition, Orlando, FL, USA, IMECE2005-82484, 2005.

[10] Kang, Y.T., Chen, W., and Christensen, R.N., "A generalized component design model by combined heat and mass transfer analysis in NH_3-H_20 absorption heat pump systems," *ASHRAE Transactions: Symposia*, p. 444-453, 1997.

[11] Cullion, R.N., Mouchka, G.A., Pence, D.V., Liburdy, J.A., and Kanury, A.M., "Ammonia desorption in microscale fractal-like branching flow networks," Proceedings of ASME HT-FED2004: Heat Transfer-Fluids Engineering Summer Conference, Charlotte, NC, USA, HT-FED2004-56660, 2004.

[12] Dence, A.E., Nowak, C.C., and Perez-Blanco, H., "A transient computer simulation of an ammonia-water heat pump in cooling mode," *Proceedings of the Intersociety Energy Conversion Engineering Conference*, vol. 2, p. 1041-1046, 1996.

[13] Fernàndez-Seara, J., and Vàzquez, M., "Study and control of the optimal generation temperature in NH_3-H_20 absorption refrigeration systems," *Applied Thermal Engineering*, vol. 21, pp. 343-357, 2001.

[14] Garimella, S., Lacy, D., and Stout, R.E., "Space-conditioning using triple-effect absorption heat pumps," *Applied Thermal Engineering*, vol. 17, pp. 1183-1197, 1997.

[15] Herold, K.E., Radermacher, R., and Klein, S.A., Absorption Chillers and Heat Pumps, CRC press, Boac Raton, 1996.

[16] Keen, S.C., and Schwartz, E.M., "Development and application of the proportional-integral-derivative control algorithm," *Journal of Undergraduate Research,* vol. 7.

[17] Skogestad, S., "Simple analytic rules for model reduction and PID controller tuning," *Journal of Process Control*, vol. 13, p. 291-309, 2003.

[18] Takeshita, K., Amano, Y., Hashizume, T., Takei, T., and Tomizawa, Masao., "Influence of refrigerant mass fraction in the performance of an ammonia absorption refrigerator," *JSME International Journal*, vol. 47, pp. 242-248, 2004.

[19] Zhu, Y., Multivariable System Identification For Process Control, Elsevier Science, Oxford, 2001.

[20] Ibrahim, O.M., and Klein, S.A., "Thermodynamic properties of ammonia-water mixtures," *ASHRAE Transactions: Symposia,* vol. 99, pp. 1495-1502, 1993.

[21] El-Shaarawi, M.A.I., and Al-Nimr, M.A., "Equations for use with computers to evaluate the performance of NH3-H2O intermittent solar refrigerators," *Energy Convers. Mgmt,* vol. 30, pp. 315-327, 1990

[22] Figliola, R.S., and Beasley, D.E., Theory and Design for Mechanical Measurements, Third Ed., John Wiley & Sons, New York, 2000.

[23] Ziegler, J.G., and Nichols, N.B., "Optimum settings for automatic controllers," *Tran. A.S.M.E.*, vol. 64, pp. 759-768, 1942.

APPENDICIES

APPENDIX 1. EXPERIMENTAL APPARATUS COMPONENT LIST

Table A1: Oil Sub-Loop Components

No.	Component	Manufacturer	Model	Quantity
1	Heat Transfer Oil	Paratherm	NF	-
2	Hot oil bath	Thermo Electron	Neslab EX7	1
3	Pump Drive	Cole Palmer	EW-75211-50	1
4	Pump Head	Micropump	75225-00	1
5	Oil Filter	Swagelok	SS-4F-40	1
6	Needle valves	Ideal Valve	V-54-2-11	2
7	Ball valve	Sharpe	58876	5
8	Flow Meter	Flow Technology	FTO-3NIXABGHC-1	1
9	Stainless Steel Tube	Swagelok	SS-T4-S-035	-
10	Fittings	Swagelok	Various, all stainless	-
11	"	Upchurch	P-713	2
12	Thermocouple	Therm-X	TR-120TT-T116-FG-2.5-STR	4
13	Pressure Transducer	Cole Parmer	68848-36	1
14	"	Cole Parmer	68848-28	1

Table A2: Ammonia-water sub loop components

No.	Component	Manufacturer	Model	Quantity
15	Strong Solution	Univar	30% Ammonia-Water	-
16	Pump	Baldor	CL3504	1
17	Surge Tank	AA Tanks	FX 200 V	1
18	Bladder Tank	AA Tanks	FMV 10	1
19	Air filter	Rti Eliminator	3P-060-M02-FI	1
20	Ammonia filter	Shelco	FOS-784-316	1
21	Ball Valve	Apollo	CF8M	1
22	Liquid needle valve	Ideal Valve	V-54-1-11	2
23	Vapor needle valve	Ideal Valve	V-54-2-11	1
24	Vapor Solenoid Valve	Burkert	6022	1
25	Valve Control Electronics	Burkert	1094	1
26	Flow Meter	Micromotion	476702	2
27	Cold water bath	Hart Scientific	7320	1
28	Building air regulator	ARO	CQ493-600-2	1
29	Bladder air regulator	ControlAir	Type 700	1
30	Cold water pump	March Mfg.	BC-3C-MD	1
31	Stainless Steel Tube	Swagelok	SS-T4-S-035	-
32	Polypropylene Tube	McMaster-Carr	5392K33	-
33	Fittings	Omega Engineering	U-06372-30	-
34	RTD Temperature Sensor	Omega Engineering	PR-10-3-100-1/8-4-E-ST	4
35	Thermocouple	Therm-X	TR-120TT-T116-FG-2.5-STR	1
36	Pressure Transducer	Omega Engineering	PX212-030 AV	3
37	Pressure Transducer	Omega Engineering	PX212-200 AV	1

Table A3: Data acquisition components

No.	Component	Manufacturer	Model	Quantity
38	Multimeter	Keithly	2001 Multimeter	1
39	RTD Reader	Keithly	2001-TSCAN	1
40	Data acquisition board	National Instruments	PCI-6043E	2
41	Terminal blocks	National Instruments	SCB-68	2
42	GIPB Interface Board	National Instruments	NI PCI-GPIB, NI-488.2	1

APPENDIX 2. CALIBRATION PROCEDURES FOR THE SOLENOID VALVE CONTROLLER

Step 1

1. Turn switch S 1-8 to ON to deactivate the zero-point switching
2. Apply 0 V to the valve control signal input
3. Using a pressure transducer and water filled syringe, apply a higher than operational pressure to the valve (24 psi)
4. With resistor R1 starting turned all the way counter-clockwise, turn R1 until flow just starts.
5. Resistor R1 is now set

Step 2

1. Start with R2 turned all the way counter-clockwise
2. Apply 10 V to the valve control signal input
3. Run the desorber at higher than normal vapor production rates by reaching steady state at the following operating conditions
    a. Oil flow rate: 650 g/min
    b. Strong solution flow rate: 45 g/min
4. With the ball valve to the solenoid valve closed, build the manifold pressure to 24 psi using the vapor needle valve
5. Keep inlet flow rate and hold up volume constant throughout this step
6. Open the ball valve to the solenoid valve and close the ball valve to the vapor needle valve

7. Watch the pressure drop once the manifold pressure drop stops, turn R2 clockwise until the pressure doesn't drop any more
8. Repeat steps 2.4 thru 2.7 with the new R2 value, continue repeating the steps until the pressure drop stops at a manifold pressure of approximately 18 psi
9. Turn switch S 1-8 to OFF to activate the zero-point switching

APPENDIX 3. INSTRUMENT AND PARAMETER UNCERTAINTY

Table A4: Instrument Uncertainty Information

Instrument Label	Description	Repetitions	Replications	U_B	Units
Temperature					
T16	TC - Upstream manifold	250	1	0.21	K
T17	TC - Downstream manifold	250	1	0.21	K
T1	RTD - Inlet AW sol'n	100	3	0.24	K
T10	RTD - Outlet AW sol'n	100	3	0.21	K
Pressure					
P2	Inlet AW sol'n	250	1	0.052	bar
P7	Saturation Pressure	250	1	0.004	bar
P9	Outlet AW sol'n	250	1	0.077	bar
Oil Flow Rate					
F13	Oil flow meter: 120°C	250	1	3.65	g/min
F13	Oil flow meter: 130°C	250	1	3.64	g/min
Density					
ρ3	Density - Inlet	250	1	0.59	kg/m^3
ρ11	Density - Outlet	250	1	0.59	kg/m^3

Table A5: Representative test parameter uncertainty values

Symbol	Value	Mean	Units
F3	Inlet mass flow rate	.0013	kg/s
ρ3	Inlet Density	0.59	kg/m^3
ρ11	Outlet Density	0.59	kg/m^3
v3	Inlet Sp. Volume	7.41E-07	m^3/kg
v11	Outlet Sp. Volume	7.06E-07	m^3/kg
P2	Inlet Pressure	0.052	bar
P9	Outlet Pressure	0.077	bar
P7	Manifold Pressure	0.0047	bar
T16	Oil Temperature	0.23	K
F13	Oil Mass Flow Rate	0.429	kg/s
f*	Rectified Circulation Ratio	0.38	-

APPENDIX 4. EXPERIMENTAL LOOP OPERATING PROCEDURES

Start-up

The warm up procedure is intended to safely begin bring the desorber to testing conditions

1. Turn the oil bath on, and allow it to come up to the desired test temperature. The oil bath should be on long enough that the internal temperature is stable.
2. Note: The bath can be controlled by an internal sensor or a sensor close to the flow meter. For warm-up, the bath should be controlled by the internal temperature.
3. Adjust the oil sub-loop ball valves so that the test manifold is bypassed.
4. Turn on the pump to approximately 500 g/min flow rate, and allow the oil sub-loop to come up to temperature. Change the bath to be controlled by the flow loop sensor, and allow it to come up to temperature.
5. Confirm the bladder tank is full and pressurized
6. Open the data acquisition program.
7. Open the ammonia-water inlet ball valve and allow solution flow into the desorber.
8. Keep the solenoid valve open (about 6 volts), and keep the exit solution need valve nearly closed to gather a hold up volume in the manifold.

9. Begin the data acquisition program.
10. Once the hold up volume level approaches the height of the desorber disk, adjust oil sub-loop ball valves so that hot oil flows through the desorber.
11. Note: Bubbles and jets will occur as the ammonia-water boils.
12. Tighten the liquid exit valve to maintain an exit solution flow rate slightly lower than the inlet solution flow rate to maintain the hold up volume.
13. Adjust the voltage to the solenoid valve using the LabVIEW™ data acquisition program to reach and maintain the desired manifold pressure.
14. Adjust the strong solution and oil to the desired flow rates.
15. Repeat steps 12 – 14 until the oil flow rate, manifold pressure, strong solution flow rate, and weak solution flow rate each reach their respective desired values in that order.

Testing

Once at steady state, data collection for a given system identification or controller verification test can begin.

System Identification Testing

The system identification tests are designed to vary the oil flow rate while maintaining a constant pressure to record how the rectified circulation ratio is changed.

1. In the LabVIEW™ data acquisition program activate the PID valve control to maintain the manifold pressure at the desired set point.
2. Once the system as been operating at stead state evidenced by temperatures remaining constant for approximately 4 minutes, begin the system identification test.
3. Activate the system identification test switch in the LabVIEW™ data acquisition program to begin the test.
4. During the test the pump voltage will be controlled by the program and will switch between two set points randomly. The pressure controller with automatically adjust the solenoid valve voltage to maintain a constant manifold pressure throughout the test.
5. During the test adjust the weak solution needle valve to maintain a constant hold up volume. An absolutely constant hold up liquid level is not critical to the test accuracy.
6. The test length is approximately 65 minutes.
7. Once the test is complete another test may be started or the shut-down procedures may be followed.

Controller Verification Testing

1. Follow the start-up procedures

2. Set the desired rectified circulation ratio for beginning the test in the controller and activate the controller.
3. Wait until the system reaches steady state at the desired rectified circulation ratio (5-15 min).
4. Begin the test by activating the desired f* tracking path or by introducing a disturbance into the system.

Shut-down

Shut-down procedure is intended to safely stop the experiment without overheating or overflowing the manifold.

1. Adjust the oil sub-loop ball valves so that the test manifold is bypassed.
2. Immediately open the liquid exit valve all the way.
3. Slow the strong solution to approximately 10 g/min.
4. Turn off oil bath and pump
5. Allow the strong solution to cool the desorber, and when all boiling has ceased, turn off strong solution at the ball valve.
6. Allow all ammonia to drain out of the manifold.
7. Open exit valves all the way, and disconnect the quick disconnect fitting at the strong solution test manifold inlet.

8. Pump water with several 60 ml syringes into the desorber to flush out the desorber disk.

9. Reconnect the strong solution inlet.

APPENDIX 5. DERIVATION OF RECTIFIED CIRUCLATION RATIO , EQUATION (12)

Derivation of $f^* = \frac{0.99 - x_3}{x_1 - x_3}$, see figure A.1 and figures 1.2 and 3.1.

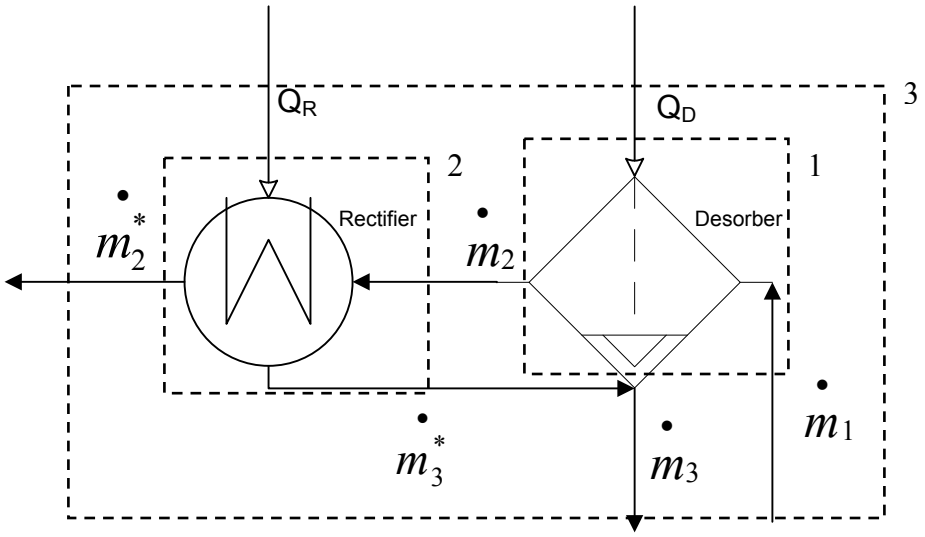

Figure A.1: Schematic of desorber rectifier system with stream labeling notation

The ammonia mass balance for the desorber, control volume 1, is

$$x_1 \dot{m}_1 = x_2 \dot{m}_2 + x_3 \dot{m}_3 \tag{A-1}$$

With the circulation ratio as:

$$f = \frac{\dot{m}_1}{\dot{m}_2} \tag{A-2}$$

the circulation ratio can be written in terms of the concentrations

$$f = \frac{x_2 - x_3}{x_1 - x_3} \tag{A-3}$$

To derive equation (A3) divide equation (A1) by $x_1 \dot{m}_2$ yielding:

$$f = \frac{\dot{m}_1}{\dot{m}_2} = \frac{x_2}{x_1} + \frac{x_3 \dot{m}_3}{x_1 \dot{m}_3} \tag{A-4}$$

Dividing the mass balance of the control volume by $\dot{m}_2$ yields:

$$f = \frac{\dot{m}_1}{\dot{m}_2} = 1 + \frac{\dot{m}_3}{\dot{m}_2} \quad \rightarrow \quad \frac{\dot{m}_3}{\dot{m}_2} = f - 1 \tag{A-5}$$

Substituting (A5) into (A4) gives the result

$$f = \frac{\dot{m}_1}{\dot{m}_2} = \frac{x_2}{x_1} + \frac{x_3}{x_1}(f - 1)$$

$$f\left(1 - \frac{x_3}{x_1}\right) = \frac{x_2 - x_3}{x_1}$$

$$f = \frac{x_2 - x_3}{x_1 - x_3}.$$

The similar procedure can be used for the desorber/rectifier system, by expanding the analysis to include control volumes 2 & 3, see figure A1.

Using control volume 3, define the rectified circulation ratio f* as:

$$f^* = \frac{\dot{m}_1}{\dot{m}_{2^*}} \tag{A-6}$$

A useful expression for $\dot{m}_{2^*}$ is derived from the mass balance and ammonia mass balance of control volume 2.

$$\dot{m}_{2^*} = \dot{m}_2 - \dot{m}_{3^*} \quad \rightarrow \quad \dot{m}_{3^*} = \dot{m}_2 - \dot{m}_{2^*} \tag{A-7}$$

and

$$x_{2^*}\,\dot{m}_{2^*} = x_2\,\dot{m}_2 - x_{3^*}\,\dot{m}_{3^*}\,. \tag{A-8}$$

Substituting (A7) into (A8)

$$x_{2^*}\,\dot{m}_{2^*} = x_2\,\dot{m}_2 - x_{3^*}\left(\dot{m}_2 - \dot{m}_{2^*}\right)$$

$$\left(x_{2^*} - x_{3^*}\right)\dot{m}_{2^*} = \left(x_2 - x_{3^*}\right)\dot{m}_2$$

$$\dot{m}_{2^*} = \frac{\left(x_2 - x_{3^*}\right)}{\left(x_{2^*} - x_{3^*}\right)}\dot{m}_2\,. \tag{A-9}$$

Substituting (A9) into (A6) yields

$$f^* = \frac{\dot{m}_1}{\frac{(x_2 - x_{3^*})}{(x_{2^*} - x_{3^*})}\dot{m}_2}$$

$$f^* = \frac{(x_{2^*} - x_{3^*})\dot{m}_1}{(x_2 - x_{3^*})\dot{m}_2}$$

$$f^* = \frac{(x_{2^*} - x_{3^*})}{(x_2 - x_{3^*})} f$$

$$f^* = \frac{(x_{2^*} - x_{3^*})}{(x_2 - x_{3^*})} \frac{x_2 - x_3}{x_1 - x_3}. \tag{A-10}$$

Assuming $x_{3^*} \approx x_3$ as described in Chapter 4 equation (A10) simplifies to the report result.

$$f^* = \frac{x_{2^*} - x_3}{x_1 - x_3} \tag{A-11}$$

APPENDIX 6. EES LIQUID AMMONIA CONCENTRATION

CALCULATION PROCEDURE "AWX_PROC"

```
PROCEDURE awx(Tin,Pin,vin: x,q,h)

"Iterates thru NH3H2O procedure for all possible concentrations to find the mass fraction of the liquid given T(K), P(bar), and v(m^3/kg)"

xlo=0
xhi=.4
dx=.0005
e=.0001E-3
x:=xlo

Repeat
    x:=x+dx
    CALL NH3H2O(123,Tin,Pin,x: T,P,x,h,s,u,v,q)
    res:=abs(v-vin)
Until(res<e)

END

CALL awx(Tin,Pin,vin: x,q,h)
```

APPENDIX 7. DERIVATION OF MATLAB LIQUID CONCENTRATION EQUATION

[5], Equation (28)

$$v_m^L = x v_a^L + (1-x) v_w^L + v^E \tag{A-12}$$

x is the ammonia mole fraction, v is the molar volume, and each term in the above equation is nondimensional.

From (21) in [5] the nondimensional form of v^E is

$$v^E = \left[\frac{\partial G_r^E}{\partial P_r} \right]_{T_r, x} \tag{A-13}$$

From (15) in [5] G_r^E is

$$G_r^E = \left[F_1 + F_2(2x-1) + F_3(2x-1)^2 \right](x - x^2) \tag{A-14}$$

which simplifies to

$$G_r^E = (F_1 - F_2 + F_3)x + (-F_1 + 3F_2 - 5F_3)x^2 + (8F_3 - 2F_2)x^3 - 4F_3 x^4 \tag{A-15}$$

Therefore (AX-2) & (AX-4) give

$$\begin{aligned} v^E = \left[\frac{\partial G_r^E}{\partial P_r} \right]_{T_r, x} &= (F_1^{'} - F_2^{'} + F_3^{'})x + (-F_1^{'} + 3F_2^{'} - 5F_3^{'})x^2 \\ &+ (8F_3^{'} - 2F_2^{'})x^3 - 4F_3^{'} x^4 \end{aligned} \tag{A-16}$$

where $F_i^{'} = \dfrac{\partial F_i}{\partial P_r}$ for $i = 1, 2, 3$. Equations (16 – 18) from [5] & [12] are:

$$F_1 = E_1 + E_2 P_r + (E_3 + E_4 P_r) T_r + \frac{E_5}{T_r} + \frac{E_6}{T_r^2}$$

$$F_2 = E_7 + E_8 P_r + (E_9 + E_{10} P_r) T_r + \frac{E_{11}}{T_r} + \frac{E_{12}}{T_r^2}$$

$$F_3 = E_{13} + E_{14} P_r + \frac{E_{15}}{T_r} + \frac{E_{16}}{T_r^2}$$

Which after differentiating give

$$F_1^{'} = E_3 + E_4 T_r \tag{A-17}$$

$$F_2^{'} = E_8 + E_{10} T_r \tag{A-18}$$

$$F_3^{'} = E_{14} \tag{A-19}$$

Equations (AX-5) thru (AX-8) give the result

$$\begin{aligned} v^E &= (E_2 - E_8 + E_{14} + (E_4 - E_{10}) T_r) x \\ &+ (-E_2 + 3E_8 - 5E_{14} - (5E_4 - 3E_{10}) T_r) x^2 \\ &+ (8E_{14} - 2E_8 - 2E_{10} T_r) x^3 - 4E_{14} x^4 \end{aligned} \tag{A-20}$$

From [5] & [12] the non-dimensional equations for v_a^L & v_m^L are

$$v_a^L = a_{a1} + a_{a2} P_r + a_{a3} T_r + a_{a4} T_r^2$$

$$v_w^L = a_{w1} + a_{w2} P_r + a_{w3} T_r + a_{w4} T_r^2$$

Which when substituted into (AX-1) along with (AX-9) results in

$$\begin{aligned} v_m^L &= (a_{w1} + a_{w2} P_r + a_{w3} T_r + a_{w4} T_r^2) \\ &+ \begin{bmatrix} E_2 - E_8 + E_{14} + (E_4 - E_{10}) T_r + (a_{a1} - a_{w1}) \\ + (a_{a2} - a_{w2}) P_r + (a_{a3} - a_{w3}) T_r + (a_{a4} - a_{w4}) T_r^2 \end{bmatrix} x \\ &+ (-E_2 + 3E_8 - 5E_{14} - (E_4 - 3E_{10}) T_r) x^2 \\ &+ (8E_{14} - 2E_8 - 2E_{10} T_r) x^3 - 4E_{14} x^4 \end{aligned} \tag{A-21}$$

MATLAB Liquid Concentration Code Listing

```
% this code calculates the ammonia mass fraction of a liquid mixture
based
% on the work done by Ibrahim. It uses a newton rhapson method to
iterate
% from the initial guess to the correct value. It has approximately
0.25%
% error from the values calculated in EES. Keith Davis 4/24/2007

% y - mole fraction, x - mass fraction, r - reduced variables, MW -
% molecular weight, some of this notation is different than what
Ibrahim
% uses in his paper.

% set tolerance for convergence of X (ammonia mass fraction)
tol=.00001;

% set constants
R=8.314; %KJ/(Kmole*K)
% reference temperature & Pressure (Ibrahim paper)
Tb=100; %K
Pb=10; %bar
% Molecular weights of ammonia=(1) & water=(2) (Herold Absorption
book
% p.26)
MW1=17.031; %g/mol
MW2=18.015; %g/mol

% Coeffiecients from Ibrahim Paper (Table 1) (1)=ammonia, (2)=water
A1=[3.971423e-2 -1.790557e-5 -1.308905e-2 3.752836e-3];
A2=[2.748796e-2 -1.016665e-5 -4.452025e-3 8.389246e-4];

% Coeffiecients from Ibrahim Paper (Table 2) (Gibbs Excess Energy
Function)
E=[-41.733398 0.02414 6.702285 -0.011475 63.608967 -62.490768
1.761064 0.008626 ...
      0.387983 -0.004772 -4.648107 0.836376 -3.553627 0.000904
24.361723 -20.736547];

% Guess ammonia mass fraction for calculations
x = 0.27;
% Convert Pressure and temperature to SI units
P_si = p*.068948; %pa units of bar
T_si = t+273.15; %ta units of K

% calculate the molecular weight from the guessed mass fraction
MW = 1/(x/MW1 + (1-x)/MW2);
% caluclate the mole fraction of ammonia from molecular weight
%x=(X/MW1)*MW; this step is not really needed
```

```
% non-dimensionalize T & P as done in Ibrahim paper
Tr = T_si/Tb;
Pr = P_si/Pb;
% get specific volume from measured density
v = 1/rho; %v units of m^3/kg

% set dummy variable dif which will be the convergence of X
dif = 1;

while dif > tol;
   % Ibrahim paper equation (8), the 100 is added to take care of
units and
   % the v*MW is to convert from specific volume to molar volume.
   V = v*MW*Pb*100/(R*Tb); % no units

   %See my thesis explanation and Ibrahim equations (21) & (15) thru
(18)
   C(1) = -4*E(14);
   C(2) = 8*E(14)-2*E(8)-2*E(10)*Tr;
   C(3) = 3*E(8)+3*E(10)*Tr-5*E(14)-E(2)-E(4)*Tr;
   C(4) = A1(1)-A2(1)+(A1(2)-A2(2))*Pr+(A1(3)-A2(3))*Tr+(A1(4)-
A2(4))*Tr^2+E(2)+E(4)*Tr-E(8)-E(10)*Tr+E(14);
   C(5) = A2(1)+A2(2)*Pr+A2(3)*Tr+A2(4)*Tr^2-V;

   % find the roots of the polynomial C
   r = roots(C);
   % check each of the possible roots
   for i = 1:length(r)
      if isreal(r(i))
         if r(i)<=1
            % set xroot to be the one real root less than 1, the new
mole
            % fraction of ammonia
            y_new = r(i);
         end
      end
   end

   % calculate the molecular weight from the new mole fraction
   MW = (y_new*MW1+(1-y_new)*MW2);
   % calculate a new mass fraction from the new molecular weight
   x_new = y_new*MW1/MW;
   % Check the difference between iterations on the mass fraction
   dif = abs(x-x_new);
   % update the mass fraction for the next iteration
   x = x_new;

end
% report the calculated mass fraction
xfin = x;
```

APPENDIX 8. SYSTEM IDENTIFICATION TEST A MODEL FITS

Table A6: Modeling fits for operating conditions A identification test

Model Name	Pecent Fit
P0	18.23
P0D	70.42
P1	64.87
P1Z	67.24
P1DZ	85.82
P1IZ	65.17
P1DIZ	87.05
P1D	86.35
P1DI	27.1
P1I	18.38
P2	72.54
P2Z	77.29
P2DZ	87.91
P2IZ	14.7

Model Name	Pecent Fit
P2DIZ	46.7
P2D	87.55
P2DI	32.4
P2I	25.4
P2U	78.42
P2ZU	83.54
P2DZU	88.66
P2IZU	79.61
P2DIZU	90.05
P2DU	88.3
P2DIU	29.25
P2IU	25.29
P3	76.93
P3Z	81.71

Model Name	Pecent Fit
P3DZ	89.12
P3IZ	67.11
P3DIZ	88.58
P3D	87.96
P3DI	30.11
P3I	18.06
P3U	84.42
P3ZU	86.85
P3DZU	88.98
P3IZU	85.7
P3DIZU	88.3
P3DU	87.57
P3DIU	26.81
P3IU	18.97

APPENDIX 9. SIMULATED CONTROLLER MODEL CLOSED LOOP RESPONSES

Table A7: Closed loop responses of all controller model combinations

		Closed Looop System Response				
Controller	System	Rise Time (sec)	%OS	Settling Time (sec)	Stead State Value	Delay Estimate (sec)
A	A	168	13.1	616	1	77
AB	A	159	15.3	840	1	77
B	A	144	17.9	786	1	77
C	A	162	9.93	567	1	76.5
D	A	256	2.65	689	1	77
E	A	230	3.9	661	1	77
A	B	188	10.7	659	1	70
AB	B	178	12.6	640	1	70
B	B	163	15.2	804	1	70
C	B	184	8.63	615	1	69.5
D	B	288	1.76	495	1	70
E	B	258	2.94	683	1	69.5
A	C	259	13.8	975	1	108
AB	C	246	16.1	1300	1	108
B	C	221	20.6	1270	1	108
C	C	244	14.5	1180	1	107
D	C	403	2.55	1080	1	108
E	C	344	4.88	1060	1	108
A	D	112	28.1	885	1	74
AB	D	106	31.2	898	1	74
B	D	93.3	32.5	850	1	74
C	D	94	17.6	636	1	73.5
D	D	159	12.5	583	1	74
E	D	144	12.3	531	1	74
A	E	165	37.9	1290	1	95.5
AB	E	157	30.9	1310	1	95.5
B	E	144	35.5	1260	1	95
C	E	154	24.6	950	1	95
D	E	234	11.2	855	1	95.5
E	E	211	13.8	773	1	95